JGR Solid Earth

RESEARCH ARTICLE
10.1029/2022JB024669

Characterization of Changes in Groundwater Storage in the Lachlan Catchment, Australia, Derived From Observations of Surface Deformation and Groundwater Level Data

Mahdiyeh Razeghi[1], Paul Tregoning[2], Manoochehr Shirzaei[3], Khosro Ghobadi-Far[3], Simon McClusky[4], and Luigi Renzullo[1]

[1]Institute for Water Futures, Australian National University, Canberra, ACT, Australia, [2]Research School of Earth Science, Australian National University, Canberra, ACT, Australia, [3]Department of Geosciences, Virginia Tech, Blacksburg, VA, USA, [4]Geoscience Australia, Symonston, ACT, Australia

Key Points:

- We estimate groundwater storage variation by combining Global Positioning System (GPS) vertical displacement and groundwater level data
- Interannual variability measured by GPS vertical deformation is mainly driven by poroelasticity effect due to groundwater storage changes
- The method is able to model seasonal groundwater level fluctuation using GPS displacement measurement and storage coefficient of the aquifer

Supporting Information:

Supporting Information may be found in the online version of this article.

Correspondence to:

M. Razeghi,
M.Razeghi@anu.edu.au

Citation:

Razeghi, M., Tregoning, P., Shirzaei, M., Ghobadi-Far, K., McClusky, S., & Renzullo, L. (2022). Characterization of changes in groundwater storage in the Lachlan catchment, Australia, derived from observations of surface deformation and groundwater level data. *Journal of Geophysical Research: Solid Earth*, *127*, e2022JB024669. https://doi.org/10.1029/2022JB024669

Received 26 APR 2022
Accepted 21 NOV 2022

Author Contributions:

Conceptualization: Mahdiyeh Razeghi, Paul Tregoning, Manoochehr Shirzaei, Khosro Ghobadi-Far
Data curation: Mahdiyeh Razeghi
Formal analysis: Mahdiyeh Razeghi
Investigation: Mahdiyeh Razeghi
Methodology: Mahdiyeh Razeghi, Manoochehr Shirzaei, Khosro Ghobadi-Far
Resources: Mahdiyeh Razeghi
Software: Mahdiyeh Razeghi

Abstract Global Positioning System (GPS) deformation measurements were combined with groundwater level data to examine the spatiotemporal variability of groundwater storage in the Lachlan catchment located in central New South Wales (Australia). After correcting for effects of glacial isostatic adjustment, non-tidal oceanic and atmospheric loading as well as hydrologic loading using existing models, we show that the seasonal and interannual variability of ground deformation and hydraulic head level data, extracted using wavelet time-frequency analysis, exhibits an in-phase behavior, indicating that the observed surface deformation is the poroelastic response to groundwater pressure change in aquifer system. Combination of GPS displacement and groundwater level change enables the estimation of elastic skeletal specific storage coefficients, which were then used for estimating groundwater storage changes. The estimated groundwater storage changes clearly reflect the four climate events of the Lachlan catchment since 1996: (a) the Millennium drought over 1996–2009, (b) the 2011–2012 La Nina and two significant floods in 2012 and 2016, (c) the drought conditions from mid-2017 to late-2019, and (d) the return of La Nina conditions since early 2020. We also found annual and long-term groundwater storage variations of respectively $\sim 25 \pm 2.7$ GL and $\sim -5 \pm 0.57$ GL/yr over the period 2012–2021. Moreover, we show that groundwater level fluctuations can be predicted from GPS displacement measurements and storage coefficients with sufficient accuracy (80% correlation and 70% RMS reduction when compared in terms of seasonal cycle). This study provides essential information that can contribute to future groundwater planning, management, and control over the Australian continent.

Plain Language Summary Groundwater extraction or recharge changes the height of the Earth's surface, which can be obtained from displacement measurements derived from Global Positioning System (GPS). We combined the GPS displacement measurements over the Lachlan aquifer, located in central New South Wales (Australia), with the groundwater level change to study groundwater storage variation. The estimated groundwater storage changes reflect the major climate conditions over the area since 1996 such as the Millennium drought and the significant La Nina events in 2011 and 2020. We further analyze the aquifer response to the rainfall and found a delay ranging from 3 weeks to 2 months between the rainfall and groundwater wells levels, depending on the depth of the aquifer.

1. Introduction

As the largest freshwater resource on Earth, groundwater is a critical resource for agricultural irrigation, urban and regional living, and industrial and mining activities (Alley et al., 2002; Zektser & Everett, 2004). Consequently, an accurate assessment of groundwater changes and availability is crucial as the demand for water resources increases due to socioeconomic developments and climate change (Döll, 2009). Reliable monitoring of groundwater storage changes is essential to identify vulnerable areas experiencing groundwater shortage and to establish a sustainable water management plan, especially in arid/semi-arid areas. The monitoring supports research on groundwater-dependent ecosystems, defined as ecosystems that require access to groundwater to meet the water requirements for maintaining the communities of plants and animals, their ecological processes and ecosystem services (Clifton et al., 2007).

In Australia, an increasingly dry continent with severe climate events (Hobday & McDonald, 2014), the importance of groundwater is particularly pronounced as it is the driest inhabited continent on Earth. The limited

Validation: Mahdiyeh Razeghi
Visualization: Mahdiyeh Razeghi
Writing – original draft: Mahdiyeh Razeghi
Writing – review & editing: Mahdiyeh Razeghi, Paul Tregoning, Manoochehr Shirzaei, Khosro Ghobadi-Far, Simon McClusky, Luigi Renzullo

surface water availability across most regions affects agriculture, energy generation, cities and ecosystems (Harrington & Cook, 2014). Increasingly dry climatic conditions, and the consequent reduction in surface water over the past decades, have caused increasing pressure on groundwater resources. Groundwater is widely used as the main source of drinking water for many cities on this continent and it is also an important water source for a wide range of other purposes such as irrigation, agriculture, and industrial use (Magee, 2009). Over the past 80 years, Australian climate data shows warming over most areas (except the inland north-west), increasing rainfall over northern, central and north-western Australia, and decreasing rainfall in eastern, south-eastern and south-western Australia (Barron et al., 2011). From 1996 to 2009, Australia (the southern Murray–Darling Basin, in particular) experienced a prolonged drought—the so-called Millennium drought. For most areas, the average rainfall decreased by more than 20% (Chiew & Prosser, 2011; Van Dijk et al., 2013). These severe climate change events and rapid population growth put tremendous stress on aquifer systems, resulting in groundwater storage loss in the affected areas (Döll et al., 2012; Famiglietti, 2014).

Satellite geodetic observations can be used to monitor groundwater storage variations indirectly. The Gravity Recovery and Climate Experiment (GRACE; Tapley et al., 2004) satellites mission and its successor GRACE Follow-On (Landerer et al., 2020), have been measuring variations in Earth's gravity field caused by mass redistribution within the cryosphere, atmosphere, hydrosphere and the solid Earth. These observations, in conjunction with hydrological models which provide other water storage components such as soil moisture, have been widely used to study groundwater storage changes (e.g., Famiglietti et al., 2011; Ojha et al., 2019; Richey et al., 2015; Rodell et al., 2009; Tregoning et al., 2012). However, the main challenges regarding this data set are both the coarse spatial resolution (∼300 km) and the monthly estimates. Interferometric Synthetic Aperture Radar (InSAR) also has been widely used to study groundwater storage changes. InSAR is frequently used to measure surface deformation over aquifers due to groundwater changes as well as to study the mechanical properties of the aquifer systems (e.g., Amelung et al., 1999; Bell et al., 2008; Chaussard et al., 2013; Miller & Shirzaei, 2015; Motagh et al., 2008; Ojha et al., 2018). Global Positioning System (GPS) is another geodetic tool measuring ground deformation that can also estimate groundwater storage changes when used in conjunction with groundwater level data (Ojha et al., 2019).

Depending on the mechanisms driving the surface deformation in a region, the 3D surface displacement measurements from GPS may be caused by different processes such as glacial isostatic adjustment, atmospheric loading and various hydrologic processes. In our study area, after accounting for the effects of glacial isostatic adjustment and non-tidal atmospheric and oceanic loading, one may assume that the remaining deformation derived from GPS data is associated with two distinct hydrologic processes (see Argus et al., 2017): (a) elastic loading of Earth's crust due to changes in terrestrial water storage and (b) poroelastic deformation of Earth's surface on top of aquifers due to variation in groundwater storage. The former is described by Earth's elastic deformation by surface loads (Farrell, 1972), while the theory of poroelasticity can explain the latter, which relates the pore pressure change within the aquifer system to the corresponding surface deformation (Poland & Davis, 1969; Wilson & Gorelick, 1996).

Poroelastic deformation results from fluid pressure change in the aquifer systems due to pumping or recharge activities. In the case of aquifer recharge, whether natural or through injection, pore pressure increase causes an uplift of the Earth's surface. In the case of groundwater extraction, such as pumping, land subsidence occurs due to pore pressure decrease and aquifer system compaction (Poland & Davis, 1969; Wilson & Gorelick, 1996). Note that this is the opposite sense of the elastic loading effect, which shows subsidence as a response to an increase in water load and uplift due to unloading (Amos et al., 2014; Argus et al., 2005, 2017; Argus, Fu, et al., 2014; Argus, Peltier, et al., 2014). This is further explained schematically in Section 4.2 for the case of using GPS vertical displacement in response to surface loads and groundwater storage changes.

Moreover, while the elastic loading response of the Earth's crust happens at large spatial scales, poroelastic deformation is a much more localized effect and occurs mainly above the aquifer (see Figure 4 of Carlson et al. (2020) for a comparison of these two processes in the Central Valley, California). Thus, the surface deformation signal associated with these two hydrologic processes is characterized by distinct spatial features.

GPS deformation measurements have been used extensively to examine and monitor changes in terrestrial water storage using the elastic loading theory (e.g., Argus, Fu, et al., 2014; Argus, Peltier, et al., 2014; Argus et al., 2017; Fu et al., 2015; Han & Razeghi, 2017; Horwath et al., 2010; Ouellette et al., 2013; Razeghi et al., 2019; Van Dam et al., 2007). In these studies, GPS stations that exhibit poroelastic behavior, including those stations directly

above aquifer systems like Central Valley are excluded from the analysis so that terrestrial water storage variations causing the elastic loading can be estimated. In principle, if there is access to estimates of groundwater storage change and aquifer system mechanical properties, one could compute the poroelastic deformation above the aquifer, remove its contribution from GPS measured deformations and use the GPS residual signal to study the water storage changes using the elastic loading theory. Conversely, if one is interested in studying groundwater storage variation using surface deformation data above an aquifer system, the elastic deformation due to changes in water storage components should first be removed from the GPS time series. This paper deals with the latter case.

In this study, vertical GPS displacement over the Lachlan catchment (located in central New South Wales, Australia) and groundwater level variations are used to study groundwater storage changes. Poroelastic deformation due to groundwater storage changes in the aquifer systems is isolated from GPS vertical deformation measurements by removing effects such as non-tidal atmospheric and oceanic loading, deformation due to soil moisture changes above the aquifer systems, glacial isostatic adjustment, and elastic loading caused by hydrologic surface loads outside the aquifer system (denoted as the "far-field" loading effect). The residual vertical displacements are combined with groundwater level changes to calculate the storage coefficient and specific storage over the aquifer. Groundwater storage change during different climate events across the Lachlan catchment are assessed using the estimated storage coefficient and observed groundwater level fluctuations. We also investigate the ability of the method to predict hydraulic head level fluctuations in both time and space domains from GPS deformation estimates.

This paper is structured as follows. Section 2 describes the study area. Data sets used in this study are introduced in Section 3. The methods for estimating the mechanical properties of aquifer systems and groundwater storage changes from GPS deformation and hydraulic head level measurements are presented in Section 4. Results and numerical experiments are presented in Section 5. We investigate various issues such as groundwater recharge from precipitation, groundwater storage changes over specific climate events such as La Nina, prediction of groundwater level changes, and dependence of the storage coefficient variability to the distance between GPS stations and groundwater wells. Discussion and conclusions are presented in the last two sections.

2. Study Area

The Lachlan catchment (indicated by the blue border in Figure 1a) is located in central New South Wales, Australia. It includes a semi-arid river system, west of the Great Dividing Range (green line in Figure 1d), and forms part of the Murray–Darling Basin (yellow area in Figure 1d). It covers around 90,000 km^2, which is about 8% of the Murray–Darling Basin, stretching across four States—Queensland, New South Wales, Victoria, and South Australia, and contributes substantially to Australia's agricultural production. Wyangala Dam (indicated by WD in Figure 1a), on the Lachlan River (east to west dashed line in Figure 1a), is the Lachlan Valley's major water storage facility and provides water for town water supplies, irrigation, stock and domestic use, industry, and environmental flows. The Lachlan River begins in the Great Dividing Range, flows north-west into Wyangala Dam, and streams nearly 1,400 km across western NSW. The Lachlan River system and its floodplain are the main topographic features of the Lachlan catchment. Its elevation decreases from east to west from 1,400 to 1,465 m. The catchment experiences a considerable temperature gradient from east (cooler and wetter) to west (hotter and drier), varying from $-9°C$ in winter to $+46°C$ in summer. The average annual rainfall of the catchment varies from 860 mm in the eastern part of the catchment to around 300 mm in the western part (Kolstad, 2018).

Based on the Murray–Darling Basin Plan in 2012 (MDBA, 2012), the Lachlan Alluvium Water Resource Plan area shown by red border in Figure 1a is composed of three resource units: the Lower Lachlan Alluvium (indicated by LL in Figure 1a), the Upper Lachlan Alluvium (Figure 1b) with an area of $\sim 28,000\,km^2$, and the Belubula Alluvium (Figure 1c) covering $\sim 180\,km^2$.

The Belubula Alluvium is comprised of clay, silt, sand and gravel to a depth of less than 40 m. Its groundwater is generally unconfined/semi-confined and is hydraulically connected to the Belubula River (the dashed line within Belubula in Figure 1c). The dominant recharge processes are direct rainfall infiltration, leakage from the Belubula River and overbank floodwaters through infiltration (Kolstad, 2018).

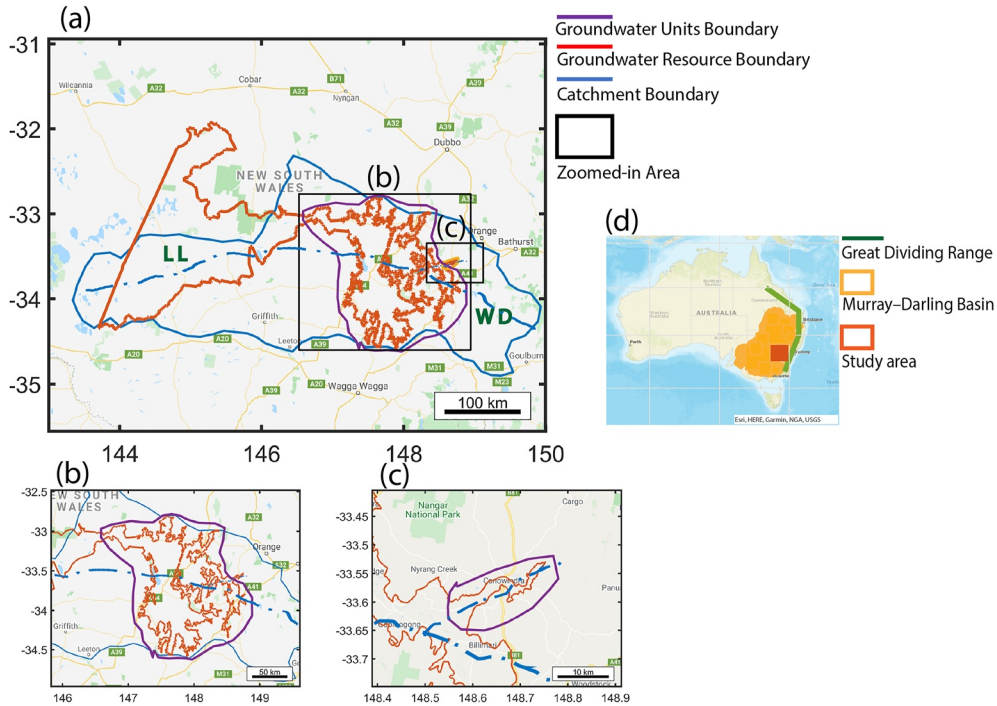

Figure 1. (a) Catchment boundary (blue border) and its groundwater unit resources Upper Lachlan and Belubula (red border). WD and LL indicate Wyangala dam and Lower Lachlan, respectively and the east to west dashed line is the Lachlan River. (b) Upper Lachlan groundwater resource within the catchment. (c) Belubula groundwater resource within Lachlan catchment. The dashed line within Belubula region is the Belubula River. (d) Study area (red rectangle), Murray-Darling Basin (yellow area), and Great Dividing Range (green line) within Australian continent.

The Upper Lachlan Alluvium includes sands and gravels within the alluvial sediments. It comprises two main aquifer systems: a shallow aquifer system to depth of between 35 and 60 m, and a deep aquifer system up to a maximum of 150 m depth. The shallow aquifer system is in a hydraulic connection with the Lachlan River. The dominant recharge processes are direct rainfall infiltration, leakage from the Lachlan River and overbank flood waters through infiltration (Kolstad, 2018).

The Lower Lachlan Alluvium is comprised of sands and gravels within the alluvial sediments. It is divided into two main aquifer systems: a shallow aquifer system to depths of between 55 and 90 m, and a deep aquifer system up to a maximum depth of 400 m. Groundwater flow direction in the deep aquifer is generally toward the west.

This study focuses only on the Belubula and Upper Lachlan, due to a sparsity of observations for the Lower Lachlan in terms of both GPS stations and groundwater wells.

3. Data Sets

We use the daily vertical GPS displacement time series provided by the Nevada Geodetic Laboratory (Blewitt et al., 2016). The displacements due to solid Earth tide and ocean tide loadings have already been removed from these measurements. Offsets due to non-geophysical and geophysical causes are corrected by fitting a linear trend, annual and semi-annual sinusoids, and a Heaviside step function applied at the offsets' epochs (http://geodesy.unr.edu/NGLStationPages/steps.txt). GPS stations' information including their 4-character ID and the corresponding coordinates are listed in Table S1 in Supporting Information S1.

To isolate changes in vertical surface deformation due to poroelastic aquifer compaction/expansion, changes induced by other effects must be removed from the observed GPS displacement. In our case study, corrections are applied to account for deformation caused by the following effects: (a) change in soil moisture load across the catchment, (b) non-tidal atmospheric and oceanic loading, (c) glacial isostatic adjustment, and (d) far-field loading effect due to terrestrial water storage changes beyond the catchment.

For the soil moisture loading correction, we use root zone soil moisture data (down to one m) provided by NASA Global Land Data Assimilation System (GLDAS) Catchment Land Surface Model (CLSM). This model is obtained from an assimilation of GRACE gravity measurement into GLDAS-2.2 CLSM, and simulations are available from 1 February 2003 (Li et al., 2019). The displacements due to soil moisture loading have been estimated using the Green's functions of elastic deformation from Farrell (1972).

The second correction is computed using non-tidal atmosphere and ocean geopotential coefficients, GAC RL06 (Dobslaw et al., 2017). The data are given in terms of spherical harmonics coefficients of geopotential, and the corresponding displacement has been calculated based on Load Love Numbers using elastic loading theory (Farrell, 1972).

We used the RL06 Center for Space Research (CSR) GRACE/GRACE-FO mascon data product for the far-field effect. Save et al. (2016) used level-1B data to construct a high-resolution global mascon solution from GRACE/GRACE-FO data. The mascon solutions provide total water storage (TWS) changes expressed in terms of Equivalent Water Height, and they are corrected for GIA using the ICE-6G_D (VM5a) model (Argus, Fu, et al., 2014; Argus, Peltier, et al., 2014; Peltier et al., 2015, 2018) and include ocean bottom pressure (GAD product) for oceanographic studies. We removed the GAD product from the CSR mascon solutions (to make them consistent with the GPS displacement in terms of signal content) and used the TWS data for the area beyond our catchment of interest. We considered a box containing the Lachlan catchment with approximately three degrees buffer as the "near-field," and the Australian continent beyond this box as the "far-field." Then, vertical elastic deformation was computed from TWS changes over the far-filed area using the Green's functions of vertical displacement and load Love numbers from Preliminary Reference Earth model (PREM) (Bevis et al., 2016; Farrell, 1972; H. Wang et al., 2012). Using a box of approximately six degrees to distinguish between the near- and far-field resulted in less than ∼5% difference in residual vertical displacement. Due to a dry climate and limited sources of surface water, the area relies mostly on groundwater (Kolstad, 2018). Therefore, soil moisture has been considered as the only hydrology signal for the near-field and loading from surface water has been treated as a negligible effect. However, using TWS changes in the far-field helps to remove the elastic loading deformation caused by all the hydrological signals beyond the catchment.

Although small in magnitude, we remove any glacial isostatic adjustment deformation in our study area using the ICE6G-D GIA model developed by Peltier et al. (2018) to be consistent with the far-field deformation effects derived from the GRACE CSR mascon solutions. We refer to Riddell et al. (2020) for a comprehensive study of GIA effects and the corresponding land motion over the Australian continent.

For the piezometric level observation, the study uses data from both the Bureau of Meteorology (BoM) of Australia, and Water New South Wales (WaterNSW). About 300 groundwater wells are available at both organizations over and around the study area. Groundwater level information are presented in terms of standing water level which is measured from the reference point on the bore (e.g., the top of casing) to the groundwater level. Positive values are below the reference point and negative values are above the reference point. The sample rate varies between the wells, from days to sub-seasonal observations, and they are available mainly from 1980.

4. Methods

4.1. Groundwater Storage Changes Using Ground Deformation and Hydraulic Head Level Data

The theory of poroelasticity relates pore fluid pressure change to the deformation of the elastic skeleton. Changes in the volume of water residing within the pore spaces can cause changes in effective stress, which manifests as aquifer compaction/expansion and land surface deformation (Poland & Davis, 1969; Wilson & Gorelick, 1996). The resultant deformation can be elastic and/or inelastic, with elastic indicating the recoverable component and inelastic resulting when the new effective stress is larger than that of the previous maximum or the so-called pre-consolidation stress. This type of deformation (compaction) is permanent.

In an aquifer system, total stress (σ_T) in any depth is (Helm, 1978):

$$\sigma_T = \sigma_e + p, \tag{1}$$

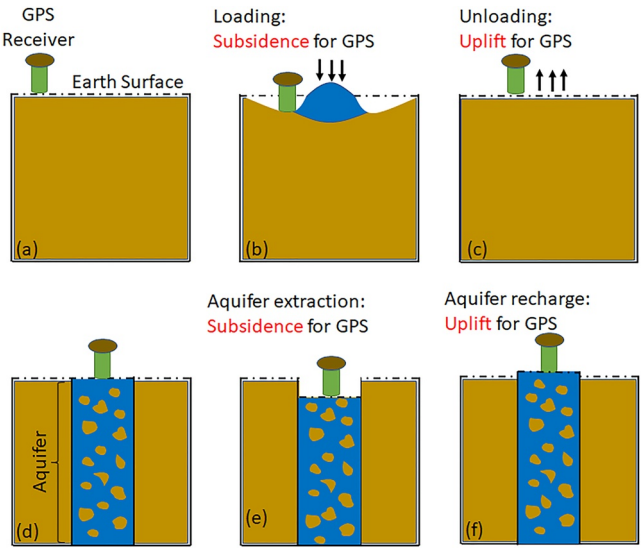

Figure 2. (a) Surface deformation response to Earth surface and underground changes: (b) Global Positioning System (GPS) reflects subsidence in response to Earth surface loading, (c) GPS shows uplift when the load is vanishing, (e) GPS response of subsidence due to aquifer extraction or pumping, and (f) GPS reflects uplift due to aquifer recharge. Panes (b and c) are associated with the elastic hydrologic loading of Earth's crust (which the black arrows are representing the direction of the load), while panels (e and f) are related to the poroelastic deformation due to groundwater storage changes above aquifers. Note that the presented deformations are not to scale.

where σ_e is the effective stress and p is pore pressure. Assuming the weight of overlying sediment is constant over time, we have (Terzaghi, 1925):

$$d\sigma_e = dp = \rho\, g\, \mathrm{d}h, \tag{2}$$

where ρ is the density of the pore water and g is the acceleration due to gravity. This means that the changes in effective stress can be determined by measuring or simulating hydraulic head (dh) variations (Poland & Davis, 1969).

Aquifer compressibility α is defined as:

$$\alpha = \frac{\mathrm{d}H}{d\sigma_e b} = \frac{\mathrm{d}H}{\mathrm{d}h\rho g b}, \tag{3}$$

where dH is the vertical change of ground deformation and b is the aquifer thickness. We use this component to estimate two important aquifer system coefficients, namely, specific storage S_s

$$S_s = \rho g \alpha, \tag{4}$$

which is the unit volume of aquifer water released from storage for a unit decline in the hydraulic head level (Lohman, 1970) or the capacity of the aquifer to release water from or take water into storage when water level changes, and storage coefficient S_k

$$S_k = S_s b, \tag{5}$$

which is volume of water taken into or released from storage per unit decline in hydraulic head, per unit area (Todd, 1980) or the percentage of pore space in the aquifer. By substituting Equations 3 and 4 into Equation 5, the storage coefficient is derived to be the ratio of ground deformation due to aquifer change to groundwater level change of the corresponding aquifer:

$$S_k = \frac{\mathrm{d}H}{\mathrm{d}h}. \tag{6}$$

The water being exchanged is derived from two processes; expansion or compression of the material that results from a change in effective stress and expansion or compression of the fluid caused by a change in pore-fluid pressure. The fluid responses will be translated from the hydraulic head of groundwater wells and the corresponding response on the surface height can be measured using GPS vertical displacement (Sneed & Galloway, 2000).

The groundwater storage (or volume) variation dV is then estimated using the storage coefficients by Davis (1982):

$$\mathrm{d}V = A \times \mathrm{d}h \times S_k = A \times \mathrm{d}h \times S_s b, \tag{7}$$

where A represents the area associated with dh over the aquifer. Note that once we compute the storage coefficient from ground deformation and groundwater level change (Equation 6), the groundwater level data alone can be used to estimate groundwater volume change (Equation 7).

4.2. GPS Response to Surface Loads and Groundwater Storage Changes

GPS measures the surface deformation response due to surface loading and poroelastic deformation above the aquifer systems. In the case of Earth elastic response to surface loads (e.g., atmospheric, oceanic, and hydrologic loading), surface deformation represents a subsidence signal due to load (Figure 2b). When the load is removed, the surface uplifts in response to the unloading (Figure 2c). In the case of groundwater storage changes, if an aquifer is experiencing water extraction (water pumping), pore pressure decreases and the aquifer will undergo compaction. The surface deformation response to compaction is subsidence (Figure 2e). In the case of aquifer recharge, pore pressure increases and the surface will uplift due to the corresponding expansion (Figure 2f).

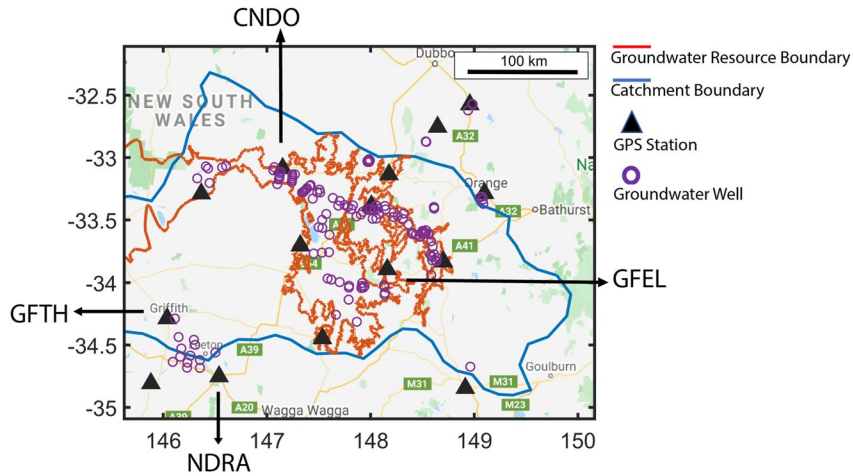

Figure 3. Data set location: 15 Global Positioning System (GPS) stations and ~300 groundwater wells over and around the Lachlan catchment, Upper Lachlan and Belubula groundwater resources. Narrandera, GFEL, and CNDO stations will be analyzed in Section 5.1 and Griffith (GFTH) station will be used in Section 5.3.

To isolate the poroelastic deformation from GPS vertical displacement in our study area, we need to remove the other effects as follows:

$$dz_{por} = dz_{GPS} - (dz_{ela} + dz_{vis}) \tag{8}$$

where dz_{por} is poroelastic deformation due to groundwater variation, dz_{GPS} is GPS vertical displacement measurement, dz_{ela} is the elastic loading deformation (which includes the non-tidal atmospheric and oceanic loading, hydrologic loading due to soil moisture in the near-field, and the elastic loading due to TWS changes in the far-field), and dz_{vis} is viscoelastic deformation attributed to GIA.

5. Results

Figure 3 shows the location of 15 GPS stations (black triangles) and ~300 groundwater wells (purple circles) over and around the study area. 8 GPS stations available over Upper Lachlan and Belubula (red boundary) within the Lachlan catchment (blue boundary) are used for estimating the groundwater storage changes. GPS deformation estimates mostly date from 2012 while groundwater levels are available from 1980.

5.1. Poroelastic Deformation

As discussed above, it is necessary to isolate the vertical displacement associated with poroelasticity from the total measured deformation. Figure 4 shows the result of this analysis for the Narrandera (NDRA) GPS station: GIA-corrected vertical displacement measurements (blue) and vertical displacement due to non-tidal atmospheric and oceanic loading (red), soil moisture loading in the near-field (yellow), and TWS loading in the far-field effects (purple). The total correction used to isolate the poroelastic deformation from GPS vertical displacement is represented by the green time series in Figure 4. The cyan time series represents the residual deformation after applying the total correction indicating poroelastic deformation due to groundwater changes. While seasonal behavior mainly characterizes the total correction from elastic loading models, the residual deformation represents seasonal and interannual variability which are likely caused by groundwater level changes in the aquifer systems. In the remainder of the paper, we refer to the residual deformation as the poroelastic deformation.

We compared the original GIA-corrected deformation and poroelastic deformation time series with nearby groundwater level data (~20–30 km away from the GPS station) for the case of three GPS stations in Figure 5: NDRA, GFEL, and CNDO. The GIA-corrected deformation measurements and poroelastic deformation are shown in blue and cyan, respectively, and groundwater level changes are shown in red. The spatial maps on the right-hand side of Figure 5 show the location of corresponding GPS stations and wells in blue rectangles. Positive values in groundwater level fluctuations indicate higher hydraulic head levels and vice-versa. As can be seen,

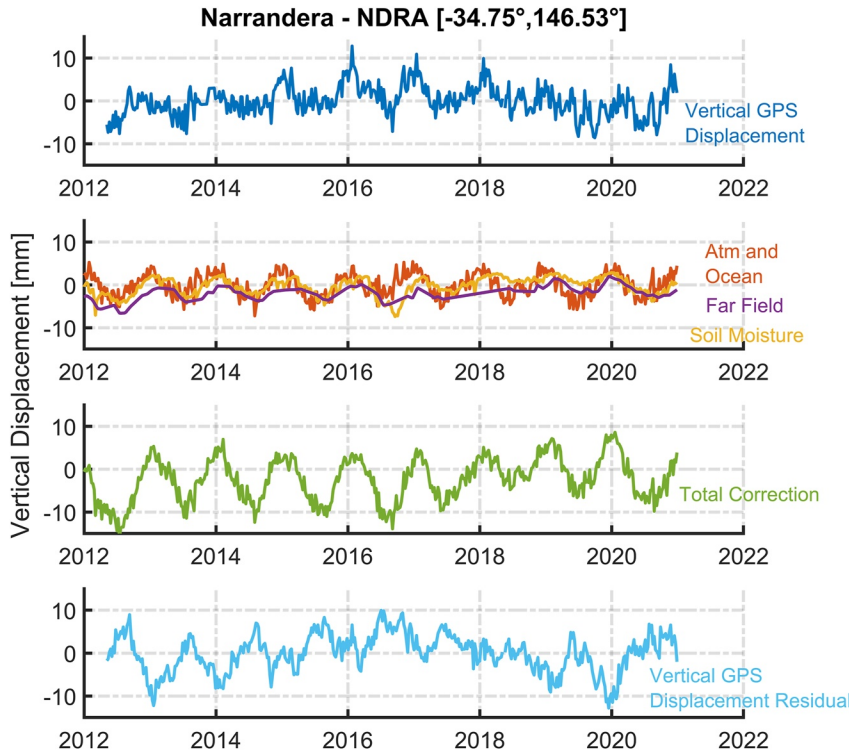

Figure 4. Isolating poroelastic deformation in Narrandera vertical Global Positioning System (GPS) displacement. Blue time series is GIA corrected vertical displacement measurement, red is displacement due to non-tidal atmospheric and oceanic loading, yellow shows the displacement due to the soil moisture loading in the near-field, and purple time series is the displacement due to total water storage loading in the far-field. Total correction in green is the summation of timeseries shown in the second panel from top. Cyan timeseries is the residual deformation obtained after removing the total correction from GIA-corrected GPS deformation. The residual displacement represents the poroelastic deformation due to groundwater changes.

the original deformation measurements and groundwater level changes do not show a notable common behavior, particularly in terms of phase. In contrast, the poroelastic deformation show an in-phase behavior with groundwater level fluctuations. The uplift (subsidence) signal is associated with an increase (decrease) in groundwater level. In addition to the clear in-phase seasonal signal, we also observe good agreement between the interannual variability in poroelastic deformation and hydraulic head level changes. For example, note the long-term subsidence and the associated drop in groundwater level from 2017 to late 2019 in the case of NDRA station. This could be related to severe drought that impacted Australia over this period (NSW Department of Planning, Industry & Environment, Lachlan Valley Snapshot 2017 to 2020 Drought). Note that although the level of agreement between poroelastic deformation and groundwater level changes is different for the three GPS stations shown in Figure 5, it is always the case that after applying the corrections, the correlation between GPS vertical deformation and groundwater level changes increases.

5.2. Time-Frequency Analysis of Seasonal Deformation and Groundwater Level

Since the time series of poroelastic deformation and hydraulic head level fluctuations (see Figure 5) are mainly characterized by seasonal behavior, we examined the agreement between the two signals at the seasonal timescale. The seasonal amplitude of deformation and groundwater level changes appear to vary from year to year, which cannot be adequately assessed using a conventional Fourier analysis. Instead, we used the continuous wavelet transform (CWT; Torrence & Gilbert, 1998) to examine the time-variable seasonal cycle in the poroelastic deformation and hydraulic head level data. Figure 6 presents the wavelet time-frequency representation (known also as spectrogram or scalogram) of the NDRA GPS station's poroelastic deformation and groundwater level changes from two nearby wells (~20 km distance between the wells and the GPS station). The wavelet

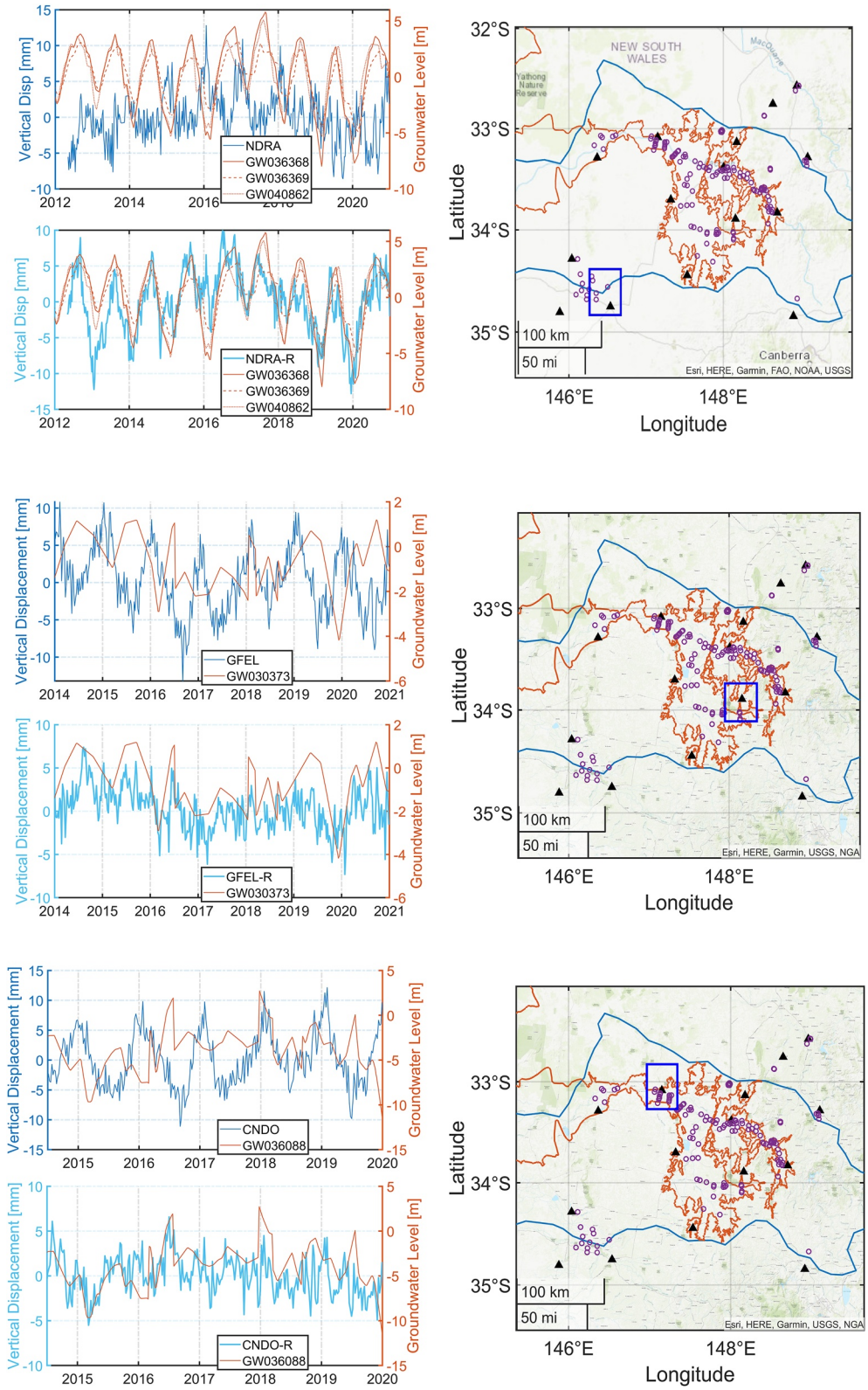

Figure 5. Comparison of vertical displacement measurements (original deformation: blue time series with 4-character ID indicating the Global Positioning System (GPS) station name; poroelastic deformation: cyan time series with 4-character ID-R) with groundwater well level change in red. The maps in the right-hand side show the location of GPS stations and the wells. The poroelastic deformations represent in-phase and similar behavior with groundwater level fluctuation.

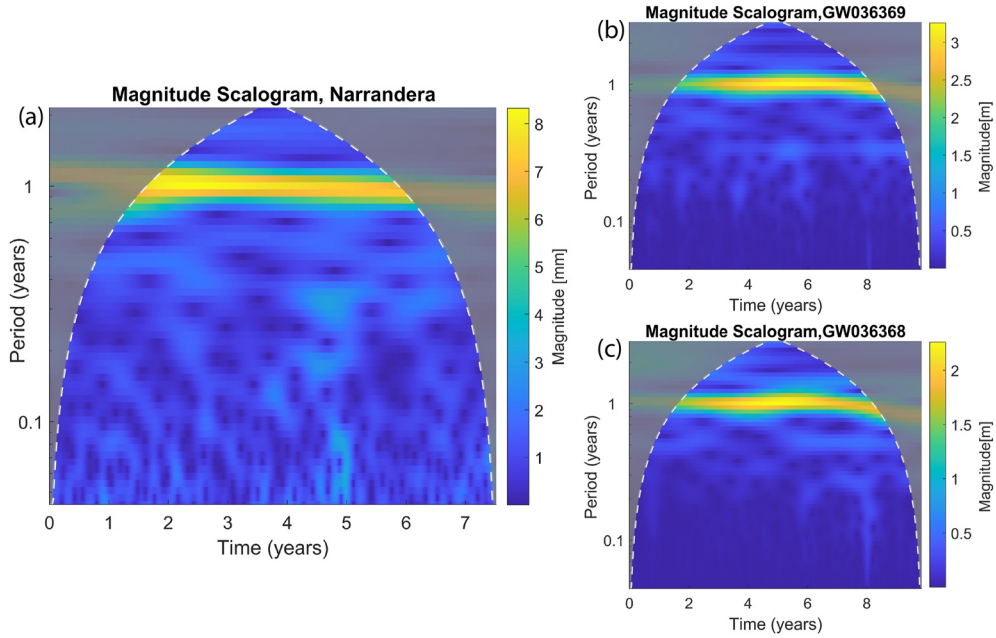

Figure 6. Time-frequency representation of (a) poroelastic deformation from Narrandera (NDRA) Global Positioning System stations and (b and c) head level changes from two nearby wells, obtained using the continuous wavelet transform. Note that all timeseries indicate a clear and large annual signal.

time-frequency representation shows that the maximum power of the signals happens at the annual timescale consistently for deformation and groundwater level data.

Applying an inverse CWT using wavelet coefficients corresponding to the period of 0.8–1.2 years (which is where the maximum power can be seen in Figure 6), we extracted the annual cycle of poroelastic deformation and hydraulic head level signals. Figure 7 compares poroelastic deformation (left panels) and its annual component extracted by inverse CWT (right panels) with hydraulic head level fluctuations from two nearby wells (GW040862 and GW036369) in top and bottom panels. The time-variable annual amplitude of both deformation and head level time series is identified using the wavelet time-frequency analysis and shows near-perfect agreement in terms of phase. Since the annual cycle of deformation and hydraulic head level changes constitutes most of the signal power and also significantly reduces the high-frequency noise (particularly in deformation time series), we used the extracted annual cycle to study the stress-strain relation between the fluid and solid variation (i.e., hydraulic head level changes vs. deformation). The results shown in Figure 7 (middle panels) reveal a relatively linear response of poroelastic deformation (obtained after applying the elastic loading corrections) to groundwater level fluctuation. The slope of the best-fitting line in this analysis represents the storage coefficient S_k (see Equation 6). The storage coefficients derived from coupling the GPS station with the two nearby groundwater wells differ by less than 3%. In the next subsection, we investigate the sensitivity of the estimated storage coefficient to the distance between GPS stations and groundwater wells and the corresponding uncertainty of different coupling scenarios.

5.3. Model Uncertainty

The aquifer system storage coefficients are estimated from pairs of GPS stations and groundwater wells using Equation 6. Depending on the distance between GPS station and the groundwater well, the variation in mechanical properties of the aquifer system over such distances results in different storage coefficients and, consequently, groundwater storage estimates. The uncertainty introduced by this effect (denoted as *model uncertainty*) is examined here.

We first considered the Griffith (GFTH) and NDRA GPS stations, separated by ~80 km, and the eight nearby groundwater wells to examine the sensitivity of storage coefficients to the pair of GPS stations and groundwater wells used for estimating them (Figure 8). Figure 8a shows the storage coefficient for each well estimated using

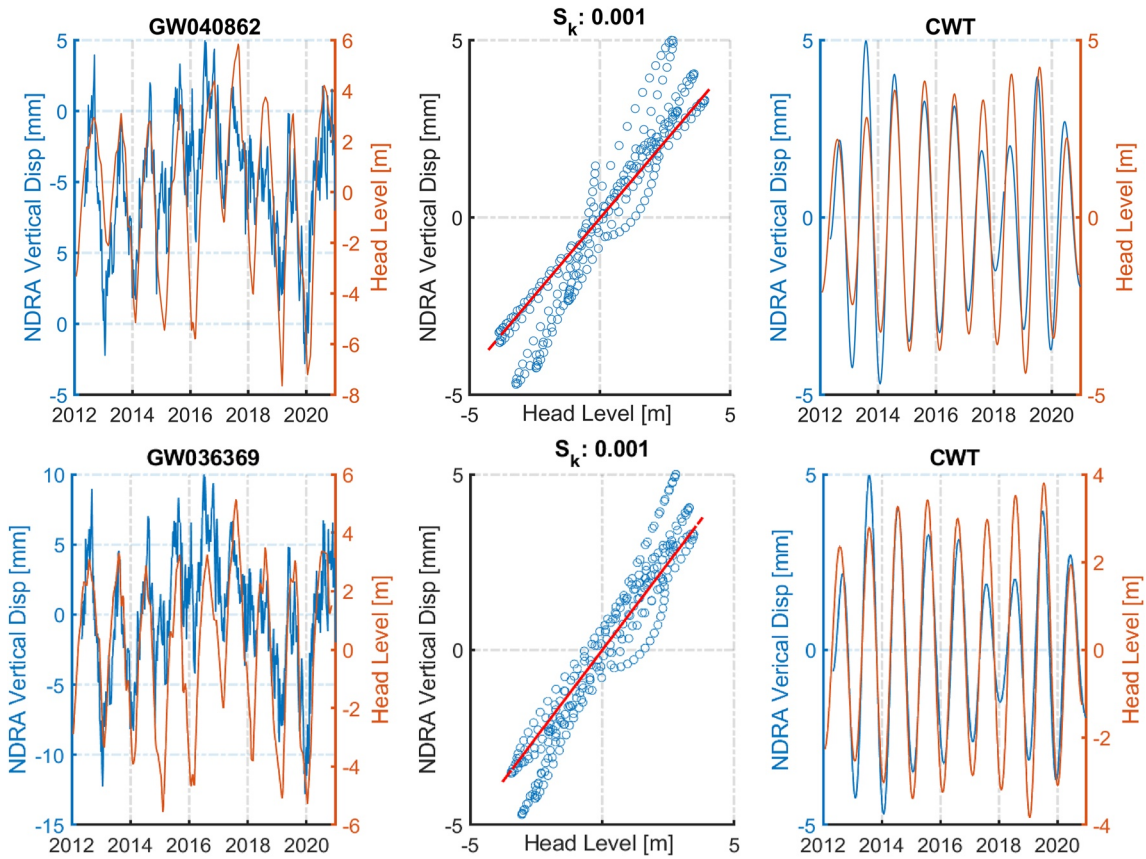

Figure 7. Comparison between poroelastic deformation from Narrandera (NDRA) Global Positioning System station (blue) and head level changes from two nearby wells (red) in top (well #GW040862) and bottom (well #GW036369) panels. The left columns show the comparison for the original signals and the rights panels show the comparison for their annual cycle extracted using continuous wavelet transform. The middle panels show the relation between annual cycle of head level changes and poroelastic deformation, with the red line indicating the best linear fit obtained using least-squares. Slope of the linear fit represents the storage coefficient S_k (see Equation 6), which is very similar for the two groundwater well data.

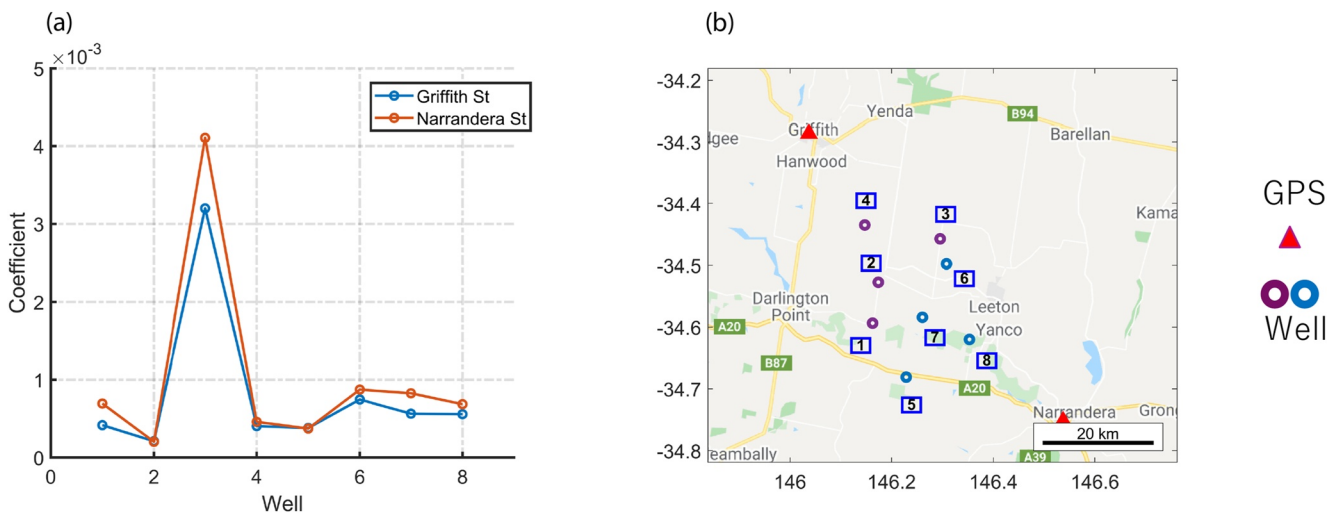

Figure 8. Comparison of the storage coefficients estimated from observations of two Global Positioning System (GPS) stations (Griffith and Narrandera) and eight groundwater wells; (a) estimated storage coefficient for each pair of groundwater well and GPS station, (b) locations of GPS stations and groundwater wells.

the poroelastic deformation from either GFTH (red line) or NDRA (blue line) GPS station. Despite varying distances from 20 to 60 km between the pairs of wells and GPS stations, we see that the estimated storage coefficients are very similar and differ by less than 10^{-14} difference (except for well #3).

As the next step, we considered four different scenarios to couple each groundwater well with one or more nearby GPS stations: (a) Using the nearest GPS station to each well or using all the GPS stations within (b) 45 km, (c) 55 km, and (d) 65 km distance from each well. Note that in scenarios (b–d) the number of estimated storage coefficients for each well is equal to the number of GPS stations considered. The storage coefficient estimated for each well in scenario (a) and the average of storage coefficients in scenarios (b–d) were then used to compute groundwater storage variations. We investigate the robustness of this approach to study groundwater in the Lachlan catchment by examining the differences among the four sets of storage coefficients and groundwater volume changes.

We estimated the storage coefficient associated with each groundwater well for the four scenarios and obtained the spatial map of storage coefficients on a regular grid of size 0.05° using a Delaunay triangulation technique combined with linear interpolation. We assumed a constant head level change of +4 m for all wells. The head level change multiplied by the corresponding storage coefficient for each well was similarly interpolated onto the same regular grid as above. Groundwater storage change was then computed by multiplying this value with the area of each grid cell (see Equation 7). Figure 9 shows the spatial maps of storage coefficients (middle panels) and groundwater storage changes (right panels). Note that the first row of Figure 9 (middle and right panels) shows the storage coefficients and groundwater storage changes for the "nearest" scenario and the last three rows represent the spatial maps of the difference between the "nearest" and other scenario. We also show the number of GPS stations used to estimate the storage coefficient for each well for different scenarios (left panels).

We see a significant variability in the number GPS stations associated with each groundwater well for different scenarios. Most of the groundwater wells in scenarios (b), (c), and (d) are coupled with 1, 2, and 3 GPS stations, respectively. Despite such notable differences among designed scenarios, the total groundwater storage variation of Upper Lachlan and Belubula for scenarios (a) to (d) are 340.88, 350.89, 345.88, and 381.00 GL, respectively, indicating a difference of ∼10%.

We also computed the standard deviation of the storage coefficient for each groundwater well from the values estimated for different scenarios and propagated them to obtain an error estimate of the groundwater storage change. The result illustrated in Figure 10 shows a maximum error of ∼ 0.2 GL, which accounts for ∼10% of the signal (similar to the difference among various scenarios presented above). These results demonstrate the robustness of the method employed in this paper to study groundwater storage variation in the Lachlan catchment. For the analyses presented in the remainder of the paper, we used scenario (a) (i.e., using the closest GPS station to each well) to estimate groundwater storage change and estimated the corresponding model uncertainty based on the standard deviation of storage coefficients obtained from the four scenarios.

5.4. Storage Coefficient and Specific Storage in the Lachlan Catchment

Combining the groundwater level fluctuations with poroelastic deformation from the nearest GPS station, aquifer system storage coefficient can be estimated using Equations 5 and 6. Figure 11 shows the spatial maps of the storage coefficient (top panel) and specific storage (bottom panel) of the Upper Lachlan and Belubula within the Lachlan catchment. To estimate specific storage, the study uses corresponding alluvium thickness, varying from 15 to 400 m, provided by Kolstad (2018) as part of a governmental report explaining the national plan for groundwater resources of Lachlan catchment. The storage coefficient shows significantly larger values in the southern region of the catchment relative to the northern part, likely indicating, among others, different mechanical properties of the aquifer system in these regions (Kolstad, 2018).

5.5. Impact of Various Climate Events on Groundwater Storage Changes in the Lachlan Catchment

We computed the catchment-averaged groundwater volume change for Upper Lachlan and Belubula. The catchment-averaged values were obtained by first multiplying the groundwater level changes with their corresponding storage coefficients, then taking the average for all the time series at each epoch, and finally scaling the obtained value with the total area of the Upper Lachlan and Belubula (28,000 + 180 km^2). The computed

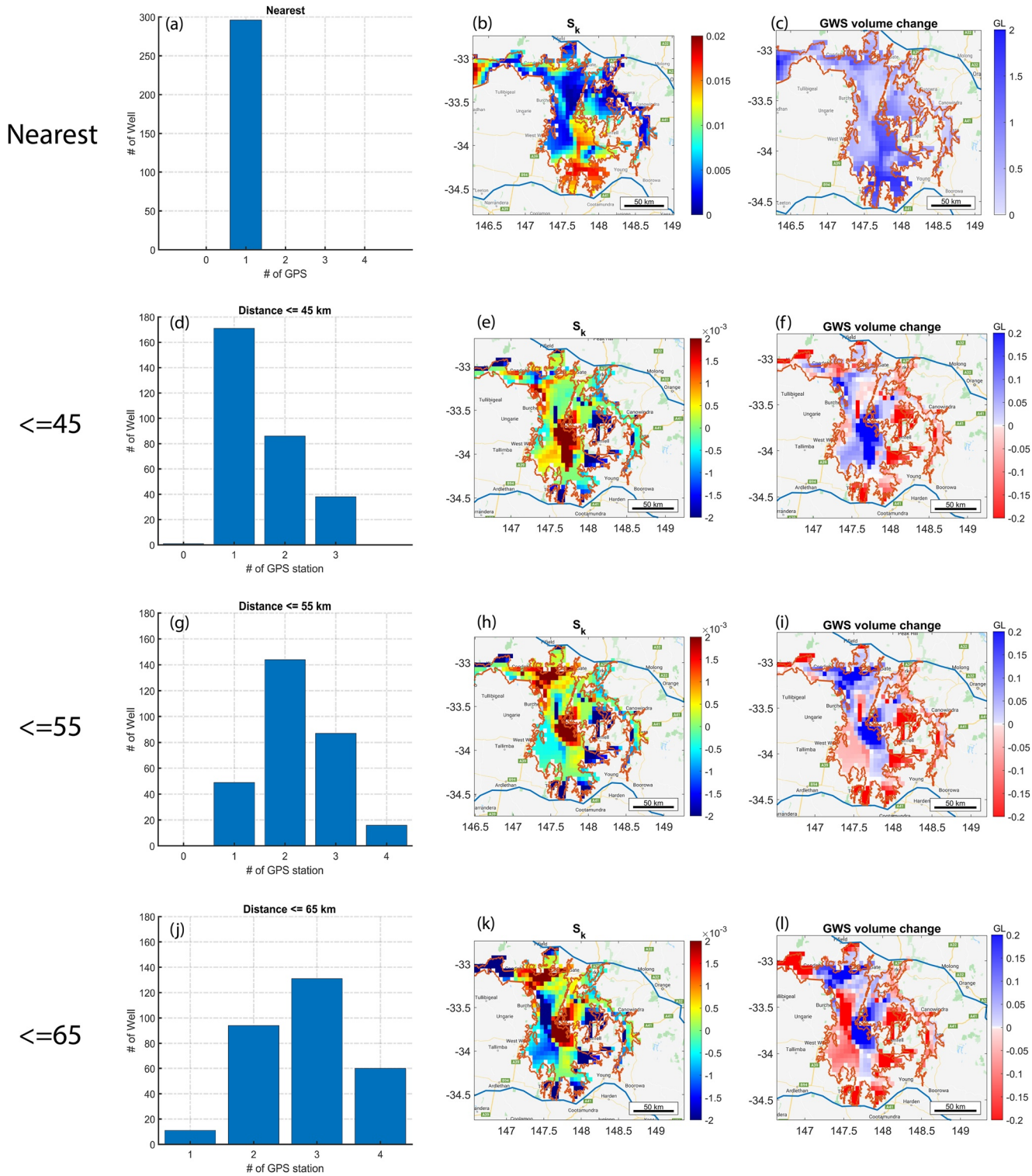

Figure 9. Left column is the number of Global Positioning System stations available for the groundwater wells in nearest scenario and their 45, 55, 65 km neighborhood (a, d, g, and j, respectively), middle column is the storage coefficient estimated over the area for the nearest scenario and using an average over each groundwater well in their 45, 55, 65 km neighborhood (b, e, h, and k, respectively), right column is the estimated groundwater storage volume change considering 4 m head level change for all of the wells in nearest and 45, 55, 65 km scenarios (c, f, i, and l, respectively). Note that the spatial maps in the middle and right columns of the last three rows are the difference between the nearest and each scenario.

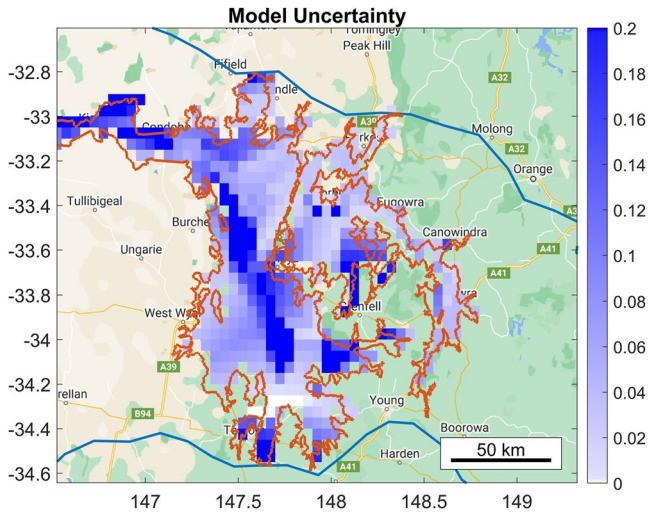

Figure 10. Model uncertainty over the area indicating the error in groundwater volume estimates due to uncertainty in computed storage coefficients. Storage coefficients uncertainty is estimated using the standard deviation of storage coefficients from four different scenarios shown in Figure 9 (coupling a well with the nearest Global Positioning System (GPS) station or all the GPS stations with 45, 55, and 65 km of the well).

timeseries of groundwater volume change from 1996 to 2021 is shown in Figure 12. The groundwater storage changes clearly show that the catchment experienced four distinct climate conditions over this period: (a) The Millennium drought (1996–2009) which was the worst drought recorded so far over the area with a period of almost 10 years without significant rainfall; (b) a La Nina in 2010–2011 and two significant floods in 2012 and 2016 which made the Wyangala Dam (the major water resource in the area) reach full capacity (Green, 2018); (c) the return of drought conditions from mid-2017 to late-2019 which put the Lachlan region's water resources under severe stress once again; and during this time, records for the whole state of NSW indicated the highest temperature and lowest rainfall (NSW Department of Planning, Industry & Environment, Lachlan Valley Snapshot 2017 to 2020 Drought); (d) In early 2020, the BoM declared La Nina conditions over the continent which causes above-average rainfall over the area (Water Allocation Statement, 2020). For the purposes of this study, 2020 to mid-2021 was considered as the second "wet era" in the region.

To obtain a more detailed evaluation of the impact of four climate events, we computed the long-term evolution of groundwater storage change over each period and then used interpolation to obtain spatial maps on a regular grid of size 0.05° (Figure 13). The long-term change was determined by calculating the trend of groundwater level change over each period multiplied by the duration of the period and then multiplied by the corresponding storage coefficient. We note that changing the grid size of interpolation to other values, such as 0.1° did not result in a notable change in the spatial maps shown here.

Figures 13a and 13b show the results for the two drought events. As expected, negative storage can be seen for both events over vast parts of the study area. The total groundwater storage loss associated with the first drought for both regions is significantly larger than the second drought; -190 ± 22 GL versus -70 ± 6.8 GL for Upper Lachlan and -0.90 ± 0.1 GL versus -0.20 ± 0.015 GL for Belubula. This may be partly due to the shorter duration of the second drought (2017–2019).

A significant storage increase can be seen in the area (Figure 13c) for the first wet event (2010–2011 La Nina and flooding in 2012 and 2016). However, the second wet era (the La Nina in the last 2 years, Figure 13d) does not replenish the area as much as the first one; 0.05 ± 0.006 GL versus 0.02 ± 0.0018 GL for Belubula and 70 ± 6.5 GL versus 15 ± 1.8 GL for Upper Lachlan, in terms of total volume change. Table 1 summarizes groundwater storage change estimates over Upper Lachlan and Belubula for the four different climate events.

5.6. Mean Seasonal Variation and Long-Term Trend of Groundwater Storage Over the Last 10 Years (2012–2021)

We also estimated the mean annual change and long-term trend of groundwater storage from GPS vertical displacement and groundwater level changes over the last 10 years (Figure 14). Since 2012, the Upper Lachlan has experienced 25 ± 2.7 GL of mean annual changes in groundwater storage, while Belubula annual groundwater storage change is $0.2 \pm 0.0.23$ GL over this period (Figure 14a). Both areas represent negative changes since 2012, showing a gradual groundwater loss of -0.02 ± 0.0026 GL/yr for Belubula and -5 ± 0.57 GL/yr for the Upper Lachlan. However, as seen in Figure 14b, a few small areas show positive trends during this period, indicating the spatial heterogeneity of long-term changes in the Upper Lachlan region. The largest negative trend over the Upper Lachlan can be seen in the Jemalong irrigation area (Figure 14b; 33.75°S, 147.75°E), which might be due to groundwater withdrawal for irrigation causing groundwater depletion. The Jemalong irrigation area covers ~900 km^2 of the region, and is a mixed farming area, with a rainfall of 432 mm/yr. The areas enterprises include prime lamb and cattle production, irrigated and dryland summer and winter cropping, and irrigated lucerne and lucerne seed production (Hill, 2000).

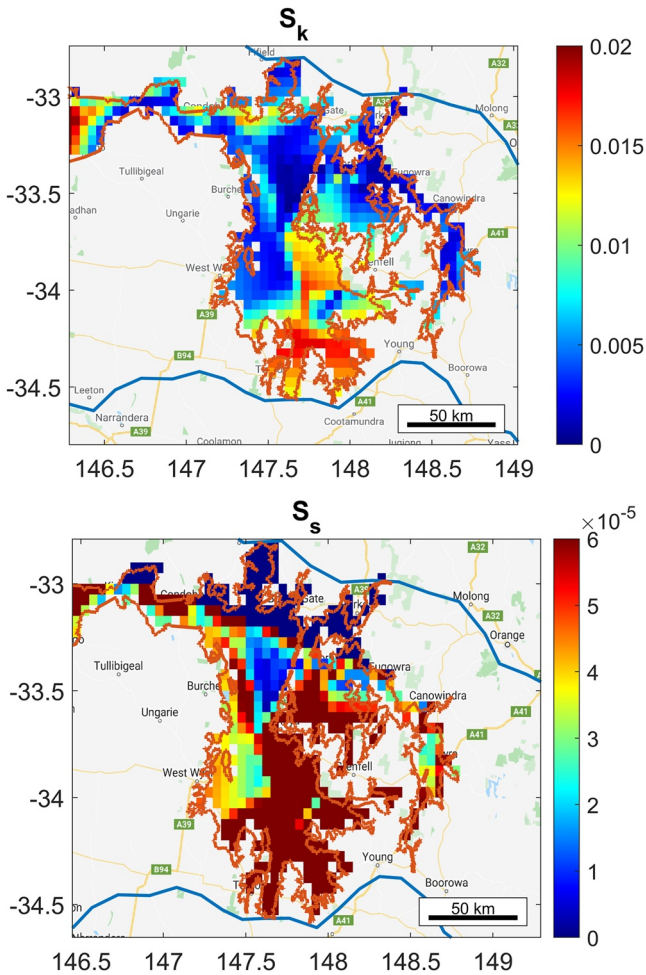

Figure 11. Spatial map of storage coefficient over the Upper Lachlan and Belubula (top) and spatial map of specific storage over the same area (bottom).

5.7. Cross-Correlation Between Groundwater Level and Precipitation

Understanding the recharge process of an aquifer can lead to better management of water resources. The main source of recharge for an aquifer is usually the infiltration of the precipitation into the ground, which is a downward flow of water, reaching the water table and adding to groundwater storage (Healy, 2010). In this section, we investigate the groundwater response to precipitation over the study area through evaluating the correlation and time lags between groundwater levels and rainfall data over the last 10 years (2012–2021).

Available data from U.S. aquifers suggest that the rates of direct percolation to unconfined aquifers is about ~600 mm/yr (McMahon et al., 2011). This rate is even slower for (semi-)confined aquifers, and in case of focused recharge that, for instance, rainfall is transformed to streamflow, the rate can be up to 80 mm/yr (Cuthbert et al., 2016). Thus, direct percolation of rainwater to the deep aquifer and recharging them over months to years is implausible (Shirzaei et al., 2019). However, rainfall can still impact deep aquifers through pressure front diffusion, propagating meters per day (H. F. Wang, 2017). Such a diffusion process is suggested for snow meltwater to propagate to a depth of ~4.5 km over ~150 days, recharging groundwater at Mt. Hood, Oregon and triggering seismicity (Saar & Manga, 2003).

For the purpose of this study, we consider three different cases over the area; Belubula with 40 m depth, shallow layer of Upper Lachlan with 60 m depth, and deep layer of Upper Lachlan with 150 m depth (see Section 2), and investigate the correlation and lags between groundwater level changes and precipitation at the three corresponding screening depths (Figure 15). We found a 3-, 5-, and 8-week delays between precipitation and peak groundwater level at wells screened at 40, 60, and 150 m depth, respectively. This diffusion time is consistent with a diffusivity of order 10^{-13} m^2/s which is consistent with the local geology (Bilge, 2012).

Figure 15 (a) gives the mean cross-correlation obtained from groundwater level data and precipitation over Belubula and shows that it takes about 3 weeks for the aquifer beneath the area (with 40 m depth) to reach maximum recharge from rainfall. This is about 5 weeks for the shallow layer of Upper

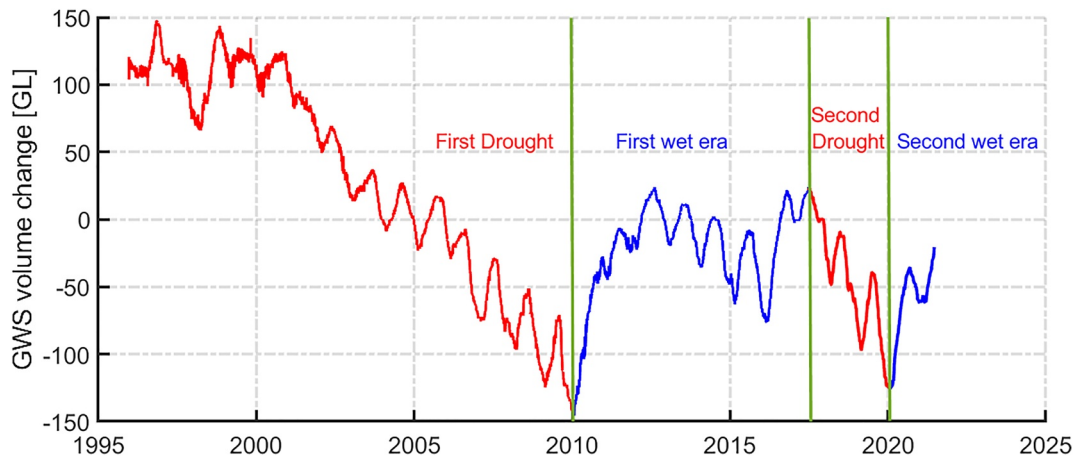

Figure 12. Basin-averaged groundwater volume change over Upper Lachlan and Belubula from 1996 to mid-2021. The time series clearly shows the four different climate condition which the catchment has experienced since 1996: first drought from 1996 to 2009, first wet period between 2010 and early 2017, second drought from 2017 to late 2019, and second wet era which started in 2020 and is still continuing.

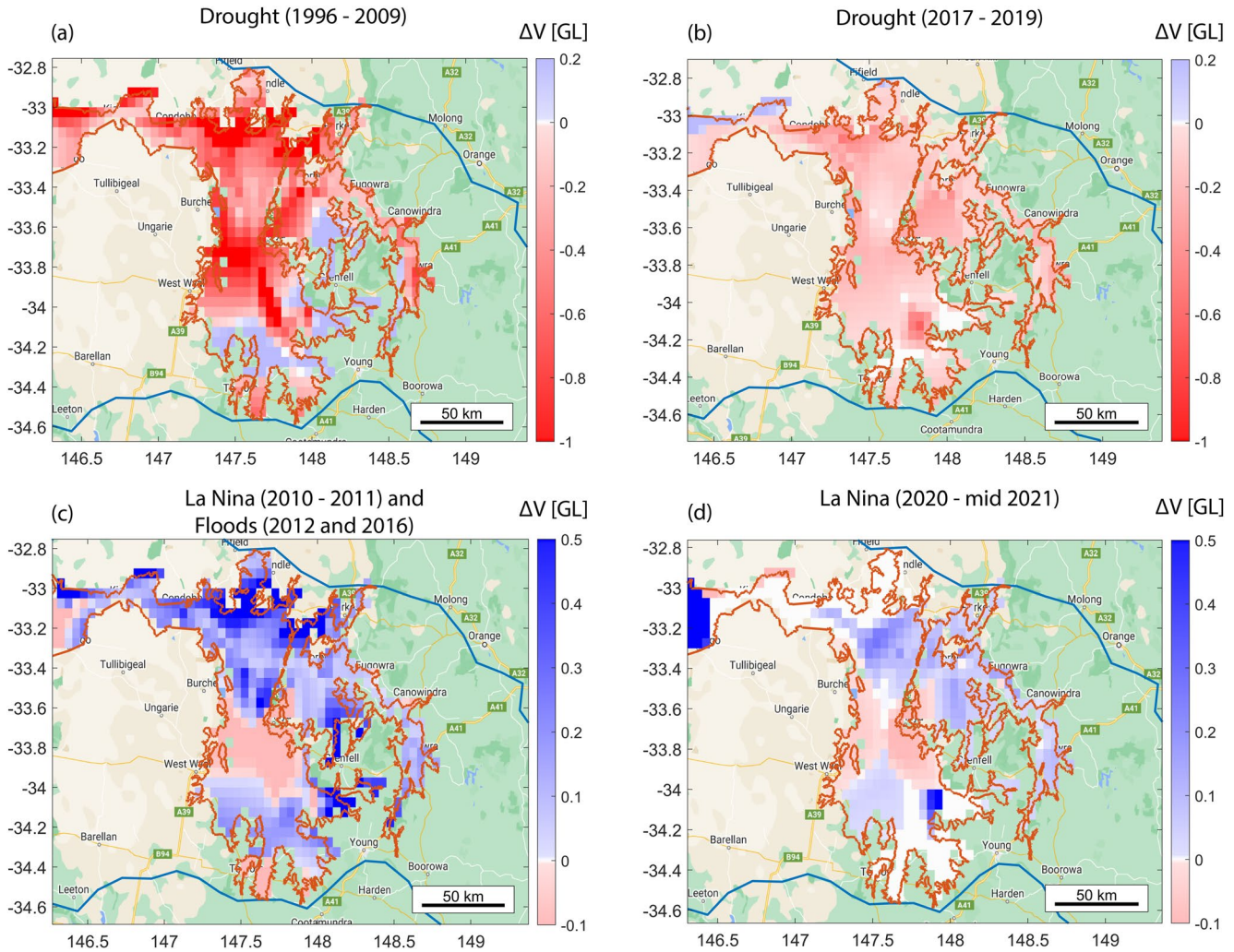

Figure 13. Groundwater storage change over the two drought periods; (a) Millennium drought (1996–2009) and (b) 2017 to 2019 drought. Upper Lachlan has experienced a volume change of −190 GL for the first drought and −70 GL for the second one, these numbers for Belubula are −0.90 and −0.20 GL for the first and second drought, respectively. Groundwater storage volume change over the two wet eras; (c) first La Nina in 2010 and 2011 plus the flooding in 2012 and 2016, and (d) current La Nina (2020 to mid-2021). Upper Lachlan has experienced a groundwater volume change of 70 GL for the first wet period and 15 GL for the second one, these numbers for Belubula are 0.05 and 0.02 GL for the first and second wet eras, respectively.

Lachlan with 60 m depth (Figure 15b) and about 2 months for the deeper layer of the aquifer (150 m depth) beneath the Upper Lachlan region (Figure 15c) in terms of responding to precipitation.

Figure 15d shows one of the groundwater wells in deep layer of Upper Lachlan (GW096088, red time series), and the precipitation over the same well (blue bar). The 2 months delay in recharge from rainfall can be clearly seen in late 2016 and mid-2017, as the peak happens for hydraulic head level change about 2 months later than the precipitation maximum. However, this is not necessarily consistent every year, as some peaks in the precipitation (e.g., early 2016) are not followed by the peak in hydraulic head level after this time.

Table 1
The Estimated Groundwater Storage Change in GL Over Upper Lachlan and Belubula for Two Droughts and Two Wet Events

Region	1996 to 2009 drought	2010 to 2016 wet era	2017 to 2019 drought	2020 to mid-2021 wet era
Upper Lachlan	−190 ± 22	70 ± 6.5	−70 ± 6.8	15 ± 1.8
Belubula	−0.90 ± 0.1	0.05 ± 0.006	−0.20 ± 0.015	0.02 ± 0.0018

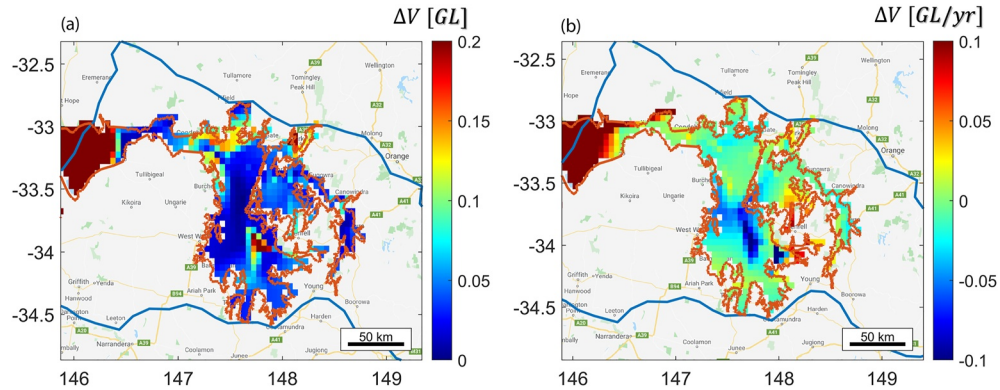

Figure 14. Groundwater storage volume change over the past 10 years (2012–2021); (a) mean annual amplitude which is 25 ± 2.7 GL for Upper Lachlan and 0.2 ± 0.0.23 GL for Belubula, (b) long-term (trend) change over the last 10 years which is negative for both areas: − 5 ± 0.57 GL/yr and − 0.02 ± 0.0026 GL/yr for Upper Lachlan and Belubula, respectively.

5.8. Prediction of Groundwater Level Changes From Surface Deformation

Groundwater level changes can be predicted (modeled) using poroelastic deformation measured by GPS and storage coefficients (see Equation 6). We first evaluated the predictability of groundwater level changes at the seasonal timescale using the seasonal cycle of poroelastic deformation extracted using CWT. To that end, data between 2012 and early 2017 were used to calculate the storage coefficient from only one pair of GPS and

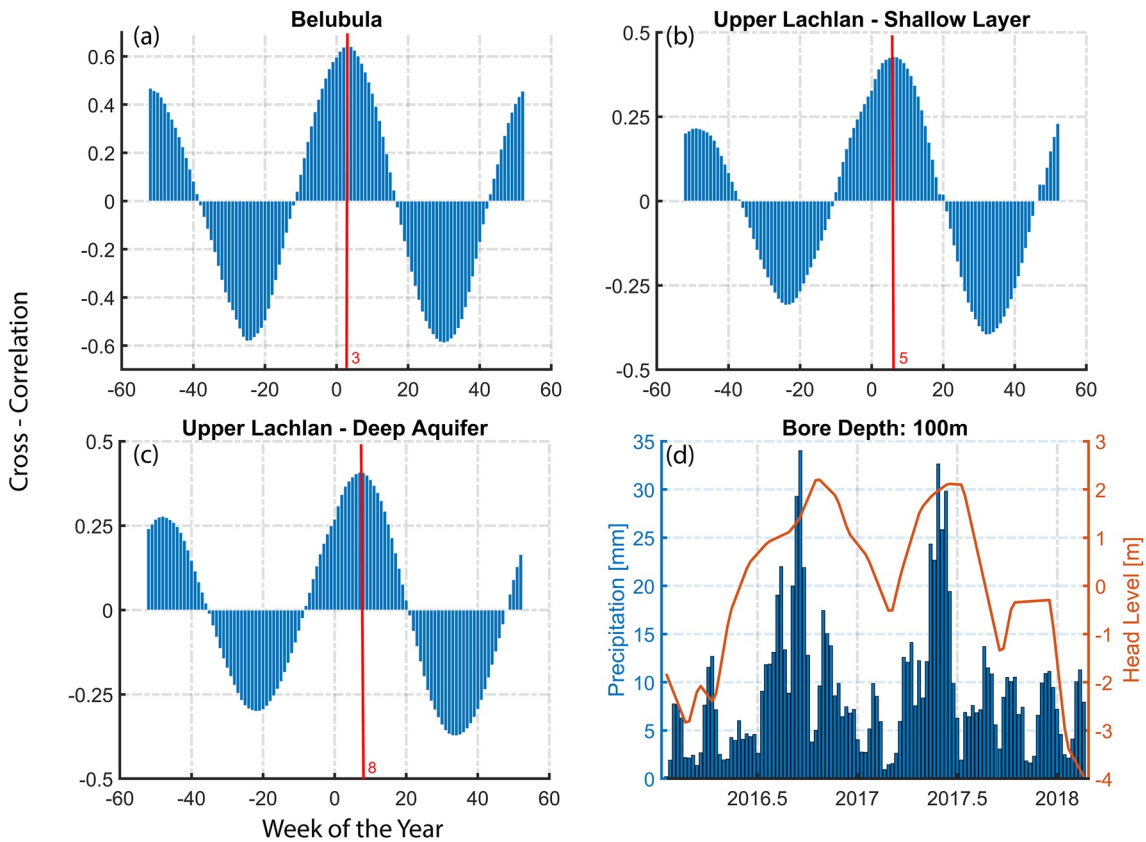

Figure 15. (a) Mean cross-correlation between groundwater wells and precipitation over Belubula, showing ~3 weeks delay for recharging from the rainfall. (b) Mean cross-correlation between groundwater wells and precipitation over shallow layers of Upper Lachlan with 60 m depth, showing ~5 weeks delay. (c) Mean cross-correlation between groundwater wells and precipitation over deep layers of Upper Lachlan with 150 m depth, showing 8 weeks delay between the well level changes and precipitation. (d) An example of groundwater level change time series (red) in the deep layer of Upper Lachlan compared with the precipitation over the area (blue bar). The 2 months delay can be seen in 2016 and 2017.

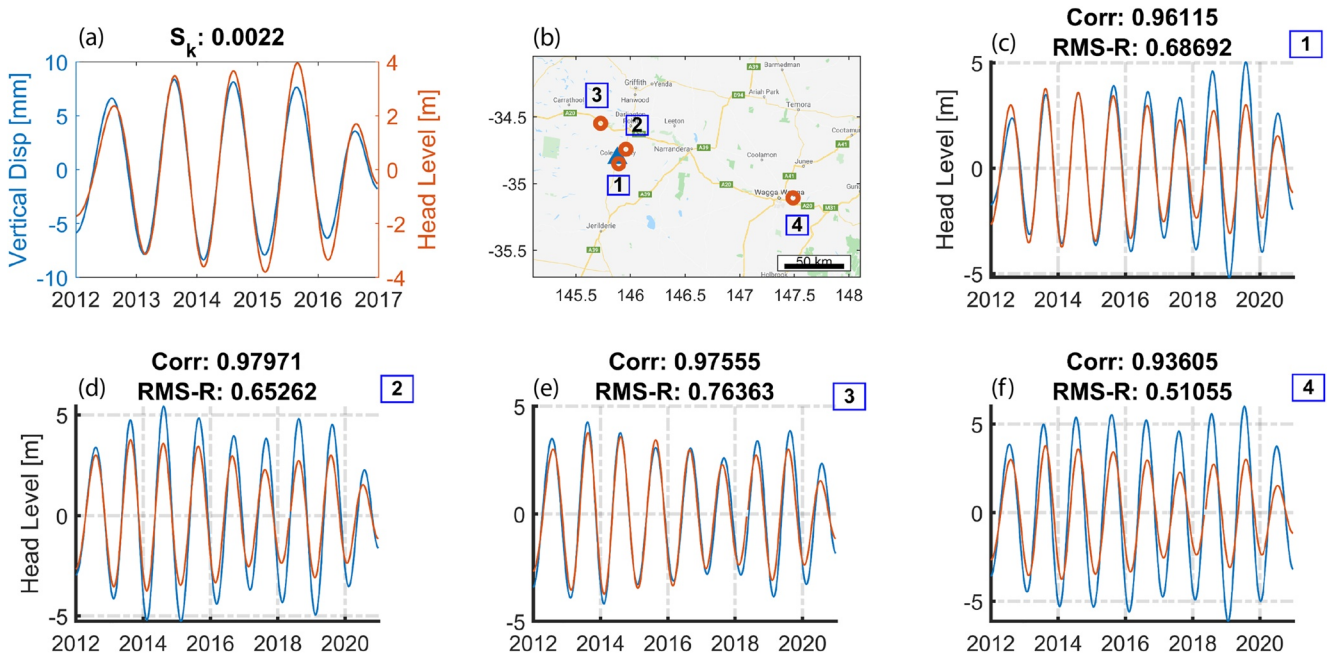

Figure 16. Prediction of the seasonal hydraulic head level change. (a) Storage coefficient calculation using data from 2012 to early 2017, using the Coleambally Global Positioning System station (blue) and GW036574 well, well number 1 (red). (b) The location of the Coleambally GPS station and nearby wells. (c) Prediction of seasonal hydraulic head level for GW036574 well (well number 1), the blue is the observed hydraulic head level change and red is the estimated using storage coefficient and GPS displacement. (d) Seasonal hydraulic head level prediction for GW030348 well, well number 2. (e) Prediction of seasonal hydraulic head level for GW030032 well, well number 3. (f) Prediction of seasonal hydraulic head level for GW036372 well, well number 4. The correlation and RMS reduction (RMS-R) between the predicted and observed groundwater level changes are also reported.

groundwater well (Figure 16a) and then we predicted the seasonal variation of hydraulic head level for another three wells within 70 km and one ~200 km distance from the GPS station between 2012 and 2021 using the seasonal variation of deformation. We evaluated the spatiotemporal reliability of our prediction in time (from 2017 to 2021) and space (within 70 km). Figure 16b shows the location of Coleambally (CLMB) GPS and wells in the area. The CLMB GPS station and the closest well (Well no. 1, GW036574) were used to calculate the storage coefficient. Figures 16c–16f compare the predicted (red) and observed (blue) seasonal variation of hydraulic head level changes for the wells nearby the CLMB GPS station.

The comparison between predicted and observed head level changes shows cross correlation larger than 90% and RMS reductions between 50% and 75% at the seasonal timescale. The predicted head level change is representing 2–3 m of error in some cases in terms of amplitude which is consistent with the ~60% RMS reduction. Although the distance of the Well no.4 (GW036372) to the GPS station is ~200 km, the method is still capable of predicting the seasonal hydraulic head level changes with 90% correlation and 50% RMS reduction.

We repeated the same analysis, using the original time series of groundwater level changes (not the annual cycle). Figure 17 shows prediction of hydraulic head level changes for Well no. 1 to 4 between 2012 and 2021. The predictions still show a high correlation (>80%) in this case; however, the RMS reduction varies over time for each well. For instance, well nos. 1 and 3 represent similar predicted and observed amplitudes between 2015 and 2018, while the difference between predicted and observed head level changes increases by ~20–30% after 2018. There are also some significant differences in terms of amplitude in 2018, 2014, and 2016 for well nos. 2, 3, and 4, respectively. This can be, among others, due to the uncertainties of storage coefficients. It is worth noting that the interannual variability in groundwater level fluctuations is accurately predicted using the poroelastic deformation measurements from GPS.

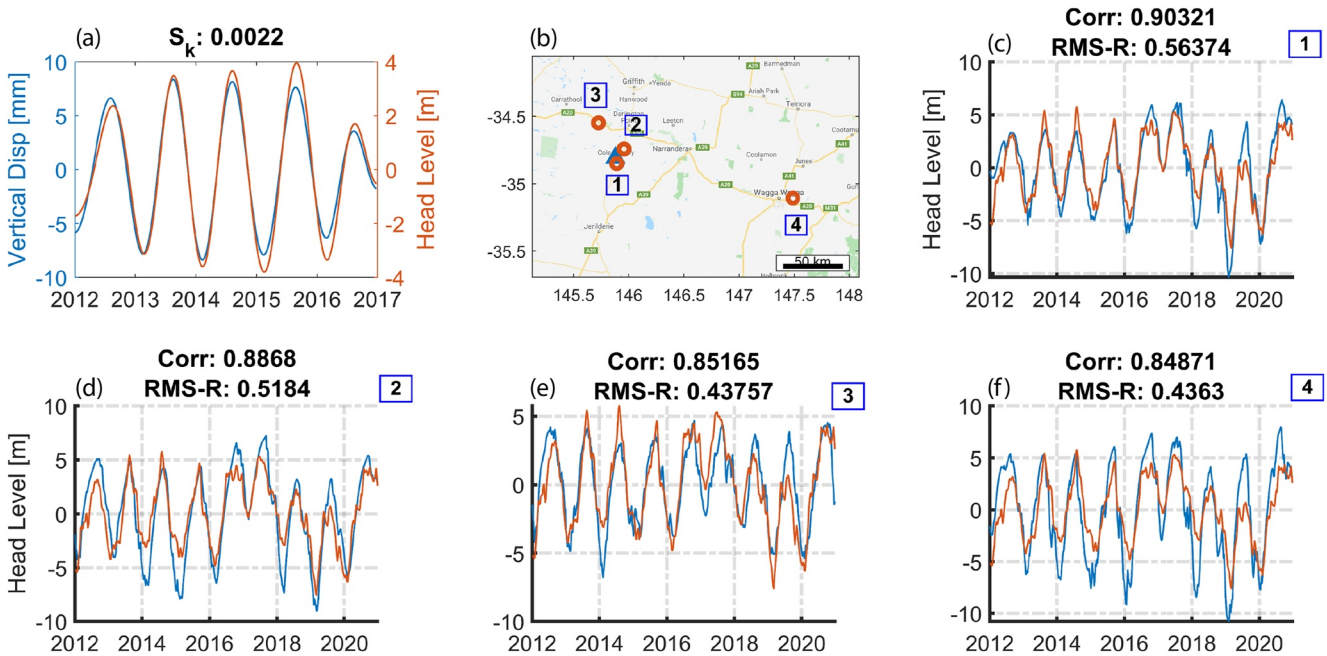

Figure 17. Same as Figure 16 but for the original groundwater level changes. As can be seen, the correlation between the observed and estimated hydraulic head level change is still high, however, the RMS reduction (RMS-R) varies over the time.

6. Discussion

6.1. Extraction of Poroelastic Deformation From GPS Displacement Measurements

This study uses the vertical deformation from GPS to estimate groundwater storage volume change over the Lachlan catchment. Since GPS-measured vertical displacement reflects the displacement due to various geophysical processes, one needs to isolate the poroelastic displacement due to groundwater changes by removing other effects using existing models and observations. In this study, we assumed that GPS vertical displacement is caused by the sum of GIA viscoelastic deformation, non-tidal oceanic and atmospheric loading, hydrologic loading by soil moisture in the near field and TWS in the far field, and poroelastic deformation due to groundwater changes. Snow and surface water components are negligible in our study area (Kolstad, 2018). Moreover, vertical deformation due to volcanic and tectonic processes is not a major effect in our case study. Depending on the study area and geophysical mechanisms deriving the vertical deformation, the set of corrections applied to extract the poroelastic deformation from GPS measurements could be very different. This should be kept in mind when trying to implement the approach we present here to other case studies elsewhere.

6.2. The Uncertainty of the Applied Corrections

The estimated groundwater storage change is dependent on the models—and their uncertainties—used to isolate the poroelastic deformation and their uncertainties. To quantify the sensitivity of our groundwater storage change estimates to the uncertainty of the corrections (Section 4.2), we employed different GIA and soil moisture models and compared the new estimate of the groundwater storage changes with the one presented above. New sets of soil moisture data from GLDAS Noah Land Surface Model (Rodell et al., 2004) and the GIA model of Caron et al. (2018) were used to isolate the poroelastic deformation. Then, the aquifer storage coefficients were estimated using the new poroelastic deformation. As the next step, basin-averaged groundwater storage changes over the area from 1996 to mid-2021 were estimated and compared with the time series given in Figure 12 (see Figure S1 in Supporting Information S1). The RMS difference between the two time series is ∼10%, demonstrating the robustness of our groundwater storage change estimation method to the applied corrections.

Since the uncertainties of models used for calculating the corrections are not known, we are not able to propagate them to estimate the uncertainly of groundwater storage estimates. Moreover, it should be emphasized that the

model uncertainty examined in Section 5.3 should be considered as a lower bound for the groundwater storage uncertainty as it does not include the impact of corrections' uncertainties.

6.3. Earth Model Uncertainty

Using Green's functions and PREM, we have calculated elastic loadings due to far-field TWS and near-field soil moisture changes. So, another potential uncertainty source can be the Earth model's choice. To quantify the impact of the selected Earth model into the groundwater storage volume change estimation, we used two additional elastic Earth models; ak135 (Kennett et al., 1995) and iasp91 (Kennett & Engdahl, 1991) and compared the results with those based on PREM. The new sets of vertical elastic deformation due to far-field TWS changes and near-field soil moisture variation were estimated using load Love numbers from ak135 and iasp91 models. Next, the aquifer storage coefficients were calculated using the new sets of poroelastic deformation and groundwater well data, and finally, the basin-averaged groundwater storage volume changes were estimated over the Lachlan catchment. The RMS difference between the time series using ak135, iasp91 and that based on PREM (Figure 12) is ∼1% which shows that the choice of Earth model has little impact on the estimation of groundwater storage volume change over the Lachlan catchment.

6.4. Elastic Loading Due To Groundwater Storage Changes

The variation of groundwater storage in the aquifer also causes elastic deformation of the Earth's crust (Holzer, 1979). This effect was not considered in the corrections used to extract the poroelastic deformation in the analysis presented above. Here, we perform a crude calculation to quantify the magnitude of this effect in the Lachlan catchment. We consider a disk load (Bevis et al., 2016) at the center of the study region with the same surface area as that of the Upper Lachlan plus Belubula and used the estimated timeseries of groundwater storage changes shown in Figure 12 to calculate the elastic deformation that is caused by the groundwater changes. The elastic deformation at the center of the disk load calculated using the PREM load Love numbers are shown in Figure S2 in Supporting Information S1. The corresponding deformation does not exceed ±0.04 mm, which shows the negligible contribution of the groundwater component in elastic load calculation over the Lachlan catchment.

6.5. Other Limitations of the Study

The accuracy of the storage coefficient estimated from vertical displacement and hydraulic head level change is affected by the uncertainty of GPS vertical deformation measurements and models used to compute the correction, as well as the pairing between GPS stations and groundwater wells. We reiterate that uncertainties of groundwater storage estimates presented here only reflect the latter (i.e., pairing between GPS stations and groundwater wells). Thus, they represent a conservative estimate or a lower bound for the groundwater storage uncertainties. Moreover, the spatial resolution of the groundwater storage change estimates is dependent on the density of GPS stations and groundwater wells over the area, which resulted in disregarding the Lower Lachlan groundwater resource area due to a huge data gap for both data sets. InSAR technique can be used to obtain a high spatial resolution deformation field covering the whole study area (e.g., Miller & Shirzaei, 2015; Ojha et al., 2018). This is a topic for future research. Also, another limitation of such studies is the undersampling of aquifer properties, which affects estimating components such as specific storage that needs accurate thickness information over the area.

7. Summary and Conclusions

We employed GPS vertical displacement time series along with groundwater head level changes to study groundwater storage variation over the two alluvium groundwater unit resources in the Lachlan catchment: Belubula and Upper Lachlan. In order to isolate the poroelastic displacement associated with groundwater storage changes, the elastic loading deformation and viscoelastic deformation were removed from GPS deformation. We demonstrated that the poroelastic deformation showed in-phase behavior with groundwater level changes at seasonal as well as interannual timescales. This analysis showed that while seasonal changes in GPS vertical deformation measurements in our study area are associated with both elastic loading (e.g., due to soil moisture and atmospheric mass)

and poroelastic effects, the interannual variability is mainly driven by poroelasticity due to groundwater storage changes.

We applied the time-frequency wavelet analysis to extract the time-variable seasonal cycle of poroelastic deformation and groundwater level changes and estimated the storage coefficient for each pair of GPS station and groundwater well. Spatial maps of storage coefficients and specific storage over the area identify a notable hydrogeology distinction between the northern and southern parts of the catchment. This is consistent with the distinct geological differences between the northern and southern parts of the Upper Lachlan catchment (Kolstad, 2018).

The average volume of groundwater storage variation for four different climate events over the area; (a) Millennium drought (1996–2009), (b) wet era of 2010–2016, (c) 2017 to 2019 drought, and (d) 2020 to mid-2021 La Nina, is ~ -0.25 and ~ -45 GL for the Belubula and the Upper Lachlan, respectively, showing that the whole area has experienced groundwater storage loss. Quantification of groundwater storage change over the past 10 years (2012–2021) for Belubula shows a mean annual variation of 0.2 ± 0.023GL and a long-term trend of $-0.02 \pm 0.0026\,\mathrm{GL/yr}$, while the Upper Lachlan has experienced 25 ± 2.7 GL of mean annual change with a long-term trend of $-5 \pm 0.57\,\mathrm{GL/yr}$ over the same period. However, due to the large area covered in the Upper Lachlan $\left(\sim 28,000\,\mathrm{km}^2\right)$, a regional investigation may result in different conclusions over different zones of this region. We note that the coarse spatial resolution (~300 km) of GRACE/GRACE-FO observations does not allow for observing the spatial variability of groundwater storage changes in the Lachlan catchment with a comparable spatial detail presented in this paper.

The mean cross-correlation between precipitation and groundwater levels at three different layers of the aquifer, Belubula with 40 m depth, shallow layer of Upper Lachlan with 60 m depth, and deep layer of Upper Lachlan with 150 m depth, reveals 3-, 5-, and 8-week delay between rainfall and peak groundwater levels, respectively.

The ability of the method to predict (model) hydraulic head level changes using poroelastic deformation from GPS timeseries was also investigated. We showed that seasonal hydraulic head level changes within an area of 70 km could be predicated with ~90% correlation and ~70% RMS reduction when compared to measured values. The prediction of original groundwater level change showed a lower accuracy with ~85% correlation and ~50% RMS reduction. This analysis showed that in addition to the time-variable seasonal cycle, the interannual variability of the groundwater level fluctuations could also be predicted with sufficient accuracy.

The results provided in this study have the potential to serve as a basis for future work focusing on the hydraulic connection of each area with the rivers and their effects on the groundwater flow (i.e., surface water—groundwater interaction), more detailed regional evaluation of the Upper Lachlan to acknowledge that different zones may present different results, and constraining the groundwater flow models of the Lachlan catchment using surface deformation measurements.

Data Availability Statement

GNSS time series were downloaded from the Nevada Geodetic Laboratory (http://geodesy.unr.edu). GRACE CSR mascon solution and the corresponding GIA grid were downloaded from http://www2.csr.utexas.edu/grace/RL05_mascons.html. The non-tidal atmosphere and ocean geopotential coefficients were downloaded from https://isdc.gfz-potsdam.de/esmdata/aod1b/. The soil moisture data from the CLSM model were downloaded from https://doi.org/10.5067/TXBMLX370XX8. The CPC precipitation data set was downloaded from ftp://ftp.cpc.ncep.noaa.gov/precip/CPC_UNI_PRCP. Groundwater level data were downloaded from the Bureau of Meteorology (http://www.bom.gov.au/water/groundwater/explorer/map.shtml) and Water New South Wales (https://www.waternsw.com.au/waterinsights/real-time-data). Basin-average groundwater storage volume change time series over Lachlan catchment (Figure 12) and long-term evolution of groundwater storage change over the area for the four climate events (Figure 13) are available at https://dx.doi.org/10.25911/xwxx-2w46.

Acknowledgments
We would like to thank the Editor Professor Isabelle Manighetti and Associate Editor Dr. Annette Eicker for handling our manuscript, and also Dr. Donald Argus and Professor Bill Hammond for their constructive and thoughtful reviews which led to a clearer presentation of our paper. Open access publishing facilitated by Australian National University, as part of the Wiley - Australian National University agreement via the Council of Australian University Librarians.

References

Alley, W. M., Healy, R. W., LaBaugh, J. W., & Reilly, T. E. (2002). Flow and storage in groundwater systems. *Science*, *296*(5575), 1985–1990. https://doi.org/10.1126/science.1067123

Amelung, F., Galloway, D. L., Bell, J. W., Zebker, H. A., & Laczniak, R. J. (1999). Sensing the ups and downs of Las Vegas: InSAR reveals structural control of land subsidence and aquifer-system deformation. *Geology*, *27*(6), 483–486. https://doi.org/10.1130/0091-7613(1999)027<0483:stuado>2.3.co;2

Amos, C. B., Audet, P., Hammond, W. C., Bürgmann, R., Johanson, I. A., & Blewitt, G. (2014). Contemporary uplift and seismicity in central California driven by groundwater depletion. *Nature*, *509*(7501), 483–486. https://doi.org/10.1038/nature13275

Argus, D. F., Fu, Y., & Landerer, F. W. (2014). Seasonal variation in total water storage in California inferred from GPS observations of vertical land motion. *Geophysical Research Letters*, *41*(6), 1971–1980. https://doi.org/10.1002/2014gl059570

Argus, D. F., Heflin, M. B., Peltzer, G., Crampé, F., & Webb, F. H. (2005). Interseismic strain accumulation and anthropogenic motion in metropolitan Los Angeles. *Journal of Geophysical Research*, *110*(B4), B04401. https://doi.org/10.1029/2003jb002934

Argus, D. F., Landerer, F. W., Wiese, D. N., Martens, H. R., Fu, Y., Famiglietti, J. S., et al. (2017). Sustained water loss in California's mountain ranges during severe drought from 2012 to 2015 inferred from GPS. *Journal of Geophysical Research: Solid Earth*, *122*(12), 10–559. https://doi.org/10.1002/2017jb014424

Argus, D. F., Peltier, W. R., Drummond, R., & Moore, A. W. (2014). The Antarctica component of postglacial rebound model ICE-6G_C (VM5a) based on GPS positioning, exposure age dating of ice thicknesses, and relative sea level histories. *Geophysical Journal International*, *198*(1), 537–563. https://doi.org/10.1093/gji/ggu140

Barron, O., Crosbie, R., Charles, S., Dawes, W., Ali, R., Evans, W., et al. (2011). *Climate change impact on groundwater resources in Australia: Summary report*. CSIRO Water for a Healthy Country Flagship.

Bell, J. W., Amelung, F., Ferretti, A., Bianchi, M., & Novali, F. (2008). Permanent scatterer InSAR reveals seasonal and long-term aquifer-system response to groundwater pumping and artificial recharge. *Water Resources Research*, *44*(2), W02407. https://doi.org/10.1029/2007wr006152

Bevis, M., Melini, D., & Spada, G. (2016). On computing the geoelastic response to a disk load. *Geophysical Journal International*, *205*(3), 1804–1812. https://doi.org/10.1093/gji/ggw115

Bilge, H. (2012). *Upper Lachlan groundwater flow model*. NSW Office of Water.

Blewitt, G., Kreemer, C., Hammond, W. C., & Gazeaux, J. (2016). MIDAS robust trend estimator for accurate GPS station velocities without step detection. *Journal of Geophysical Research: Solid Earth*, *121*(3), 2054–2068. https://doi.org/10.1002/2015jb012552

Carlson, G., Shirzaei, M., Werth, S., Zhai, G., & Ojha, C. (2020). Seasonal and long-term groundwater unloading in the Central Valley modifies crustal stress. *Journal of Geophysical Research: Solid Earth*, *125*(1), e2019JB018490. https://doi.org/10.1029/2019jb018490

Caron, L., Ivins, E. R., Larour, E., Adhikari, S., Nilsson, J., & Blewitt, G. (2018). GIA model statistics for GRACE hydrology, cryosphere, and ocean science. *Geophysical Research Letters*, *45*(5), 2203–2212. https://doi.org/10.1002/2017gl076644

Chaussard, E., Amelung, F., Abidin, H., & Hong, S.-H. (2013). Sinking cities in Indonesia: ALOS PALSAR detects rapid subsidence due to groundwater and gas extraction. *Remote Sensing of Environment*, *128*, 150–161. https://doi.org/10.1016/j.rse.2012.10.015

Chiew, F., & Prosser, I. (2011). *Water and climate* (p. 29). Science and S.

Clifton, C., Cossens, B., McAuley, C., Evans, R., Cook, P., Howe, P., & Boulton, A. (2007). A framework for assessing the environmental water requirements of groundwater dependent ecosystems.

Cuthbert, M. O., Acworth, R. I., Andersen, M. S., Larsen, J. R., McCallum, A. M., Rau, G. C., & Tellam, J. H. (2016). Understanding and quantifying focused, indirect groundwater recharge from ephemeral streams using water table fluctuations. *Water Resources Research*, *52*(2), 827–840. https://doi.org/10.1002/2015wr017503

Davis, G. H. (1982). Prospect risk analysis applied to ground-water reservoir evaluation. *Ground Water*, *20*(6), 657–662. https://doi.org/10.1111/j.1745-6584.1982.tb01383.x

Dobslaw, H., Bergmann-Wolf, I., Dill, R., Poropat, L., Thomas, M., Dahle, C., et al. (2017). A new high-resolution model of non-tidal atmosphere and ocean mass variability for de-aliasing of satellite gravity observations: AOD1B RL06. *Geophysical Journal International*, *211*(1), 263–269. https://doi.org/10.1093/gji/ggx302

Döll, P. (2009). Vulnerability to the impact of climate change on renewable groundwater resources: A global-scale assessment. *Environmental Research Letters*, *4*(3), 035006. https://doi.org/10.1088/1748-9326/4/3/035006

Döll, P., Hoffmann-Dobrev, H., Portmann, F. T., Siebert, S., Eicker, A., Rodell, M., et al. (2012). Impact of water withdrawals from groundwater and surface water on continental water storage variations. *Journal of Geodynamics*, *59*, 143–156. https://doi.org/10.1016/j.jog.2011.05.001

Famiglietti, J. S. (2014). The global groundwater crisis. *Nature Climate Change*, *4*(11), 945–948. https://doi.org/10.1038/nclimate2425

Famiglietti, J. S., Lo, M., Ho, S. L., Bethune, J., Anderson, K. J., Syed, T. H., et al. (2011). Satellites measure recent rates of groundwater depletion in California's Central Valley. *Geophysical Research Letters*, *38*(3), 2010GL046442. https://doi.org/10.1029/2010gl046442

Farrell, W. E. (1972). Deformation of the Earth by surface loads. *Reviews of Geophysics*, *10*(3), 761–797. https://doi.org/10.1029/rg010i003p00761

Fu, Y., Argus, D. F., & Landerer, F. W. (2015). GPS as an independent measurement to estimate terrestrial water storage variations in Washington and Oregon. *Journal of Geophysical Research: Solid Earth*, *120*(1), 552–566. https://doi.org/10.1002/2014jb011415

Green, D. (2018). Lachlan Surface Water Resource Plan Surface water resource description.

Han, S. C., & Razeghi, S. M. (2017). GPS recovery of daily hydrologic and atmospheric mass variation: A methodology and results from the Australian continent. *Journal of Geophysical Research: Solid Earth*, *122*(11), 9328–9343. https://doi.org/10.1002/2017jb014603

Harrington, N., & Cook, P. G. (2014). *Groundwater in Australia*. National Centre for Groundwater Research and Training.

Healy, R. W. (2010). *Estimating groundwater recharge*. Cambridge University Press.

Helm, D. C. (1978). Field verification of a one-dimensional mathematical model for transient compaction and expansion of a confined aquifer system. In *Verification of mathematical and physical models in hydraulic engineering* (pp. 189–196).

Hill, C. M. (2000). Economic evaluation of options in the Jemalong Land and Water Management Plan.

Hobday, A. J., & McDonald, J. (2014). Environmental issues in Australia. *Annual Review of Environment and Resources*, *39*, 1–28. https://doi.org/10.1146/annurev-environ-012113-111451

Holzer, T. L. (1979). Elastic expansion of the lithosphere caused by groundwater depletion. *Journal of Geophysical Research*, *84*(B9), 4689–4698. https://doi.org/10.1029/jb084ib09p04689

Horwath, M., Rülke, A., Fritsche, M., & Dietrich, R. (2010). Mass variation signals in GRACE products and in crustal deformations from GPS: A comparison. In *System Earth via geodetic-geophysical space techniques* (pp. 399–406). Springer.

Kennett, B. L., Engdahl, E. R., & Buland, R. (1995). Constraints on seismic velocities in the Earth from traveltimes. *Geophysical Journal International*, *122*(1), 108–124. https://doi.org/10.1111/j.1365-246x.1995.tb03540.x

Kennett, B. L. N., & Engdahl, E. R. (1991). Traveltimes for global earthquake location and phase identification. *Geophysical Journal International*, *105*(2), 429–465. https://doi.org/10.1111/j.1365-246x.1991.tb06724.x

Kolstad, K. (2018). *Lachlan alluvium water resource plan groundwater resource description*. NSW Department of Industry—Lands and Water. Retrieved from https://www.industry.nsw.gov.au/__data/assets/pdf_file/0010/175969/Lachlan-alluvium-appendice-a-water-resource-description.pdf

Landerer, F. W., Flechtner, F. M., Save, H., Webb, F. H., Bandikova, T., Bertiger, W. I., et al. (2020). Extending the global mass change data record: GRACE Follow-On instrument and science data performance. *Geophysical Research Letters*, *47*(12), e2020GL088306. https://doi.org/10.1029/2020gl088306

Li, B., Rodell, M., Kumar, S., Beaudoing, H. K., Getirana, A., Zaitchik, B. F., et al. (2019). Global GRACE data assimilation for groundwater and drought monitoring: Advances and challenges. *Water Resources Research*, *55*(9), 7564–7586. https://doi.org/10.1029/2018wr024618

Lohman, S. W. (1970). *Definitions of selected ground-water terms, revisions and conceptual refinements* (Water Supply Paper). US Geological Survey.

Magee, J. W. (2009). *Palaeovalley groundwater resources in arid and semi-arid Australia: A literature review*. Geoscience Australia.

McMahon, P. B., Plummer, L. N., Böhlke, J. K., Shapiro, S. D., & Hinkle, S. R. (2011). A comparison of recharge rates in aquifers of the United States based on groundwater-age data. *Hydrogeology Journal*, *19*(4), 779–800. https://doi.org/10.1007/s10040-011-0722-5

MDBA. (2012). *Assessment of environmental water requirements for the proposed Basin Plan: Great Cumbung Swamp*. Murray–Darling Basin Authority.

Miller, M. M., & Shirzaei, M. (2015). Spatiotemporal characterization of land subsidence and uplift in Phoenix using InSAR time series and wavelet transforms. *Journal of Geophysical Research: Solid Earth*, *120*(8), 5822–5842. https://doi.org/10.1002/2015jb012017

Motagh, M., Walter, T. R., Sharifi, M. A., Fielding, E., Schenk, A., Anderssohn, J., & Zschau, J. (2008). Land subsidence in Iran caused by widespread water reservoir overexploitation. *Geophysical Research Letters*, *35*(16), L16403. https://doi.org/10.1029/2008gl033814

NSW Department of Planning, Industry & Environment. *Lachlan Valley snapshot 2017 to 2020 drought*. NSW Department of Planning, Industry & Environment. Retrieved from https://www.industry.nsw.gov.au/__data/assets/pdf_file/0004/469255/Lachlan-Valley-snapshot-drought-2017-20-20210914.pdf

Ojha, C., Shirzaei, M., Werth, S., Argus, D. F., & Farr, T. G. (2018). Sustained groundwater loss in California's Central Valley exacerbated by intense drought periods. *Water Resources Research*, *54*(7), 4449–4460. https://doi.org/10.1029/2017wr022250

Ojha, C., Werth, S., & Shirzaei, M. (2019). Groundwater loss and aquifer system compaction in San Joaquin Valley during 2012–2015 drought. *Journal of Geophysical Research: Solid Earth*, *124*(3), 3127–3143. https://doi.org/10.1029/2018jb016083

Ouellette, K. J., de Linage, C., & Famiglietti, J. S. (2013). Estimating snow water equivalent from GPS vertical site-position observations in the Western United States. *Water Resources Research*, *49*(5), 2508–2518. https://doi.org/10.1002/wrcr.20173

Peltier, W. R., Argus, D. F., & Drummond, R. (2015). Space geodesy constrains ice age terminal deglaciation: The global ICE-6G_C (VM5a) model: Global Glacial Isostatic Adjustment. *Journal of Geophysical Research: Solid Earth*, *120*(1), 450–487. https://doi.org/10.1002/2014jb011176

Peltier, W. R., Argus, D. F., & Drummond, R. (2018). Comment on "An assessment of the ICE-6G_C (VM5a) glacial isostatic adjustment model" by Purcell et al. *Journal of Geophysical Research: Solid Earth*, *123*(2), 2019–2028. https://doi.org/10.1002/2016jb013844

Poland, J. F., & Davis, G. H. (1969). Land subsidence due to withdrawal of fluids. *Reviews in Engineering Geology*, *2*, 187–269. https://doi.org/10.1130/REG2-p187

Razeghi, M., Han, S. C., McClusky, S., & Sauber, J. (2019). A joint analysis of GPS displacement and GRACE geopotential data for simultaneous estimation of geocenter motion and gravitational field. *Journal of Geophysical Research: Solid Earth*, *124*(11), 12241–12263. https://doi.org/10.1029/2019jb018289

Richey, A. S., Thomas, B. F., Lo, M.-H., Reager, J. T., Famiglietti, J. S., Voss, K., et al. (2015). Quantifying renewable groundwater stress with GRACE. *Water Resources Research*, *51*(7), 5217–5238. https://doi.org/10.1002/2015wr017349

Riddell, A. R., King, M. A., & Watson, C. S. (2020). Present-day vertical land motion of Australia from GPS observations and geophysical models. *Journal of Geophysical Research: Solid Earth*, *125*(2), e2019JB018034. https://doi.org/10.1029/2019jb018034

Rodell, M., Houser, P. R., Jambor, U. E. A., Gottschalck, J., Mitchell, K., Meng, C.-J., et al. (2004). The Global Land Data Assimilation System. *Bulletin of the American Meteorological Society*, *85*(3), 381–394. https://doi.org/10.1175/bams-85-3-381

Rodell, M., Velicogna, I., & Famiglietti, J. S. (2009). Satellite-based estimates of groundwater depletion in India. *Nature*, *460*(7258), 999–1002. https://doi.org/10.1038/nature08238

Saar, M. O., & Manga, M. (2003). Seismicity induced by seasonal groundwater recharge at Mt. Hood, Oregon. *Earth and Planetary Science Letters*, *214*(3–4), 605–618. https://doi.org/10.1016/s0012-821x(03)00418-7

Save, H., Bettadpur, S., & Tapley, B. D. (2016). High-resolution CSR GRACE RL05 mascons. *Journal of Geophysical Research: Solid Earth*, *121*(10), 7547–7569. https://doi.org/10.1002/2016jb013007

Shirzaei, M., Ojha, C., Werth, S., Carlson, G., & Vivoni, E. R. (2019). Comment on "Short-lived pause in Central California subsidence after heavy winter precipitation of 2017" by KD Murray and RB Lohman. *Science Advances*, *5*(6), eaav8038. https://doi.org/10.1126/sciadv.aav8038

Sneed, M., & Galloway, D. L. (2000). *Aquifer-system compaction and land subsidence: Measurements, analyses, and simulations: The Holly site, Edwards Air Force Base, Antelope Valley, California (No. 4015)*. US Department of the Interior, US Geological Survey.

Tapley, B. D., Bettadpur, S., Watkins, M., & Reigber, C. (2004). The Gravity Recovery and Climate Experiment: Mission overview and early results. *Geophysical Research Letters*, *31*(9), L09607. https://doi.org/10.1029/2004gl019920

Terzaghi, K. (1925). Principles of soil mechanics, IV—Settlement and consolidation of clay. *Engineering News-Record*, *95*(3), 874–878.

Todd, D. K. (1980). Groundwater hydrology. In R. Tomás, et al. (Eds.), *A ground subsidence study based on DInSAR data: Calibration of soil parameters and subsidence prediction in Murcia City*. John Wiley & Sons.

Torrence, C., & Compo, G. P. (1998). A practical guide to wavelet analysis. *Bulletin of the American meteorological society*, *79*(1), 61–78. https://doi.org/10.1175/1520-0477(1998)079<0061:APGTWA>2.0.CO;2

Tregoning, P., McClusky, S., Van Dijk, A., Crosbie, R. S., & Peña-Arancibia, J. L. (2012). Assessment of GRACE satellites for groundwater estimation in Australia. *National Water Commission, Canberra*, *82*.

van Dam, T., Wahr, J., & Lavallée, D. (2007). A comparison of annual vertical crustal displacements from GPS and Gravity Recovery and Climate Experiment (GRACE) over Europe. *Journal of Geophysical Research*, *112*(B3), B03404. https://doi.org/10.1029/2006jb004335

Van Dijk, A. I., Beck, H. E., Crosbie, R. S., De Jeu, R. A., Liu, Y. Y., Podger, G. M., et al. (2013). The millennium drought in Southeast Australia (2001–2009): Natural and human causes and implications for water resources, ecosystems, economy, and society. *Water Resources Research*, *49*(2), 1040–1057. https://doi.org/10.1002/wrcr.20123

Wang, H., Xiang, L., Jia, L., Jiang, L., Wang, Z., Hu, B., & Gao, P. (2012). Load Love numbers and Green's functions for elastic Earth models PREM, iasp91, ak135, and modified models with refined crustal structure from Crust 2.0. *Computers & Geosciences*, *49*, 190–199. https://doi.org/10.1016/j.cageo.2012.06.022

Wang, H. F. (2017). *Theory of linear poroelasticity with applications to geomechanics and hydrogeology*. Princeton University Press.
Water Allocation Statement. (2020). *Water availability and allocation update*. NSW Department of Planning, Industry and Environment.
Wilson, A. M., & Gorelick, S. (1996). The effects of pulsed pumping on land subsidence in the Santa Clara Valley, California. *Journal of Hydrology*, *174*(3), 375–396. https://doi.org/10.1016/0022-1694(95)02722-x
Zektser, I. S., & Everett, L. G. (2004). *Groundwater resources of the world and their use* (IHP-VI ser. Groundwater6). United Educational Scientific and Cultural Organization.